TOWARDS UNDERSTANDING THE ROBUSTNESS OF DIFFUSION-BASED PURIFICATION: A STOCHASTIC PERSPECTIVE

Yiming Liu[1*], **Kezhao Liu**[1*], **Yao Xiao**[1], **Ziyi Dong**[1], **Xiaogang Xu**[2], **Pengxu Wei**[1,3†], **Liang Lin**[1,3]
[1]Sun Yat-Sen University, [2]Chinese University of Hong Kong, [3]Peng Cheng Laboratory
{liuym225, liukzh9, xiaoy99, dongzy6}@mail2.sysu.edu.cn
xiaogangxu00@gmail.com, weipx3@mail.sysu.edu.cn, linliang@ieee.org

ABSTRACT

Diffusion-Based Purification (DBP) has emerged as an effective defense mechanism against adversarial attacks. The success of DBP is often attributed to the forward diffusion process, which reduces the distribution gap between clean and adversarial images by adding Gaussian noise. While this explanation is theoretically sound, the precise contribution of this process to robustness remains unclear. In this paper, through empirical analysis, we propose that the intrinsic stochasticity in the DBP process is the primary factor driving robustness. To test this hypothesis, we introduce a novel Deterministic White-Box (DW-box) evaluation protocol to assess robustness in the absence of stochasticity, and we analyze attack trajectories and loss landscapes. Our results suggest that DBP models primarily rely on stochasticity to avoid effective attack directions, while their ability to purify adversarial perturbations may be limited. To further enhance the robustness of DBP models, we propose Adversarial Denoising Diffusion Training (ADDT), which incorporates classifier-guided adversarial perturbations into the diffusion training process, thereby strengthening the models' ability to purify adversarial perturbations. Additionally, we propose Rank-Based Gaussian Mapping (RBGM) to improve the compatibility of perturbations with diffusion models. Experimental results validate the effectiveness of ADDT. In conclusion, our study suggests that future research on DBP can benefit from a clearer distinction between stochasticity-driven and purification-driven robustness.

1 INTRODUCTION

Deep learning has achieved remarkable success across various domains, including computer vision (He et al., 2016), natural language processing (OpenAI, 2023), and speech recognition (Radford et al., 2023). However, in this flourishing landscape, the persistent specter of adversarial attacks casts a shadow over the reliability of these neural models. In the context of vision models, adversarial attacks involve introducing imperceptible perturbations into input images, tricking the models into producing incorrect outputs with high confidence (Goodfellow et al., 2015; Szegedy et al., 2014). This has spurred substantial research into adversarial defense (Zhang et al., 2019; Samangouei et al., 2018; Shafahi et al., 2019; Wang et al., 2023).

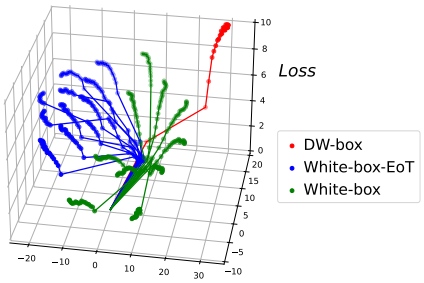

Figure 1: Comparison of attack trajectories under different evaluation settings. The attack trajectory in the standard White-box setting deviates significantly from the DW-box trajectory and shows lower effectiveness.

Recently, diffusion-based purification (DBP) (Nie et al., 2022) has emerged as a promising defense against various adversarial attacks. Existing studies suggest that DBP robustness primarily stems from the forward diffusion process, which reduces the distribution gap between clean and adversarial images by applying Gaussian noise (Nie et al., 2022; Wang et al., 2022). While this reduction is theoretically supported, its contribution to DBP robustness has not been sufficiently validated through empirical studies. Additionally,

[*]Equal contribution, [†]Corresponding author.

experimental resuts suggest that the stochastic nature of DBP might also play a significant role in enhancing its robustness (Nie et al., 2022).

In this paper, we introduce a new perspective, emphasizing the importance of stochasticity throughout the DBP process as a key contributor to its robustness, challenging the traditional focus on the forward diffusion process. To evaluate the impact of stochasticity, we propose a Deterministic White-box (DW-box) attack setting where the attacker has complete knowledge of both the model parameters and the stochastic elements. Our findings reveal that DBP models experience a significant loss of robustness when the process is made entirely deterministic from the attacker's perspective, underscoring the crucial role of stochasticity. Further analysis of attack trajectories and the loss landscape shows that DBP models do not defend against adversarial perturbations with a flat loss landscape, as seen in adversarial training (AT) (Madry et al., 2018); instead, they leverage stochasticity to bypass the most effective attack directions, as illustrated in Figure 1.

Building on this new perspective of DBP robustness, we hypothesize that it can be further enhanced by improving the diffusion model's ability to purify adversarial perturbations. To test this hypothesis, we propose Adversarial Denoising Diffusion Training (ADDT) for DBP models. This method follows an iterative two-step process: first, the Classifier-Guided Perturbation Optimization (CGPO) step generates adversarial perturbations; then, the diffusion model training step updates the parameters of the diffusion model using these perturbations. To better integrate these perturbations into the diffusion framework, we propose Rank-Based Gaussian Mapping (RBGM), which adjusts the adversarial perturbations to more closely resemble Gaussian noise, in line with the theoretical foundation of diffusion models. Experiments across various diffusion methods, attack settings, and datasets suggest that ADDT consistently enhances the robustness of DBP models. Through further empirical analysis and discussion, we argue that future research on DBP should separate the robustness derived from stochasticity and that achieved through purification. This distinction points to two complementary directions for improving DBP: (1) enhancing its ability to purify adversarial perturbations through efficient training methods, and (2) defending against Expectation over Transformation (EoT) attacks (Athalye et al., 2018b) by increasing the variance of attack gradients.

Our main contributions are as follows:

- We present a novel perspective on DBP robustness, emphasizing the crucial role of stochasticity and challenging the conventional purification-based view that robustness primarily results from reducing the distribution gap via the forward diffusion process.
- We introduce a new Deterministic White-box attack setting and show that DBP models rely on stochastic attack gradients to avoid the most effective attack directions, revealing distinct properties compared to robust models obtained through adversarial training.
- We validate that DBP robustness can be further enhanced by improving the diffusion model's ability to purify adversarial perturbations through the proposed ADDT method.

2 Related Work

Adversarial training (AT). First introduced by Madry et al. (2018), AT seeks to develop a robust classifier by incorporating adversarial examples into the training process. It has nearly become the de facto standard for enhancing the adversarial robustness of neural networks (Athalye et al., 2018a; Gowal et al., 2020; Rebuffi et al., 2021). Recent advances in AT harness the generative power of diffusion models to augment training data and prevent AT from overfitting (Gowal et al., 2021; Wang et al., 2023). However, the application of AT to DBP methods has not been thoroughly explored.

Adversarial purification. Adversarial purification utilizes generative models to remove adversarial perturbation from inputs before downstream models process them. Traditionally, generative adversarial networks (GANs) (Samangouei et al., 2018) or autoregressive models (Song et al., 2018) are employed as the purifier model. More recently, diffusion models have been introduced for adversarial purification, in a technique termed diffusion-based purification (DBP), and have shown promising results (Nie et al., 2022; Wang et al., 2022; Wu et al., 2022; Xiao et al., 2022). The robustness of DBP models is often attributed to the wash-out effect of Gaussian noise introduced during the forward diffusion process. Nie et al. (2022) propose that the forward diffusion process results in a reduction of the Kullback-Leibler (KL) divergence between the distributions of clean and adversarial images. Gao et al. (2022) suggest that while the forward diffusion process improves robustness by reducing model

invariance, the backward process restores this invariance, thereby undermining robustness. However, these theories explaining the robustness of DBP models lack substantial experimental support.

3 PRELIMINARIES

Adversarial training. Adversarial training aims to build a robust model by including adversarial samples during training (Madry et al., 2018). This approach can be formulated as a min-max problem, where it first generates adversarial samples (the maximization) and then adjusts the parameters to resist these adversarial samples (the minimization). Formally, this can be represented as:

$$\boldsymbol{\theta}^* = \arg\min_{\boldsymbol{\theta}} \mathbb{E}_{(\boldsymbol{x},y)\sim\mathcal{D}} \left[\max_{\boldsymbol{\delta}\in\mathcal{B}} L(f(\boldsymbol{\theta}, \boldsymbol{x}+\boldsymbol{\delta}), y)\right], \tag{1}$$

where L is the loss function, f is the classifier, $(\boldsymbol{x}, y) \sim \mathcal{D}$ denotes sampling training data from distribution $\mathcal{D}$, and $\mathcal{B}$ defines the set of permissible perturbation $\boldsymbol{\delta}$.

Diffusion models. Denoising Diffusion Probabilistic Models (DDPM) (Ho et al., 2020) and Denoising Diffusion Implicit Models (DDIM) (Song et al., 2020) simulate a gradual transformation in which noise is added to images and then removed to restore the original image. The forward process can be represented as:

$$\boldsymbol{x}_t = \sqrt{\overline{\alpha}_t}\boldsymbol{x}_0 + \sqrt{1-\overline{\alpha}_t}\boldsymbol{\epsilon}, \quad \boldsymbol{\epsilon} \sim \mathcal{N}(\mathbf{0}, \boldsymbol{I}), \tag{2}$$

where $\boldsymbol{x}_0$ is the original image and $\boldsymbol{x}_t$ is the noisy image. $\overline{\alpha}_t$ is the cumulative noise level at step t ($1 < t \leq T$, where T is the number of diffusion training steps) . The parameters $\boldsymbol{\theta}$ are optimized by minimizing the distance between the actual and predicted estimated noise:

$$\boldsymbol{\theta}^* = \arg\min_{\boldsymbol{\theta}} \mathbb{E}_{\boldsymbol{x}_0,t,\boldsymbol{\epsilon}} \left[\|\boldsymbol{\epsilon} - \boldsymbol{\epsilon}_{\boldsymbol{\theta}}(\sqrt{\overline{\alpha}_t}\boldsymbol{x}_0 + \sqrt{1-\overline{\alpha}_t}\boldsymbol{\epsilon}, t)\|_2^2\right], \tag{3}$$

where $\boldsymbol{\theta}^*$ represents the optimized parameters, and $\boldsymbol{\epsilon}_{\boldsymbol{\theta}}$ is the model's noise prediction. Using $\boldsymbol{\epsilon}_{\boldsymbol{\theta}^*}$, we can estimate $\hat{\boldsymbol{x}}_0$ in a single step:

$$\hat{\boldsymbol{x}}_0 = \left(\boldsymbol{x}_t - \sqrt{1-\overline{\alpha}_t}\boldsymbol{\epsilon}_{\boldsymbol{\theta}^*}(\boldsymbol{x}_t, t)\right)/\sqrt{\overline{\alpha}_t}, \tag{4}$$

where $\hat{\boldsymbol{x}}_0$ is the recovered image. DDPM typically takes an iterative approach to restore the image, removing a small amount of Gaussian noise at a time:

$$\hat{\boldsymbol{x}}_{t-1} = \left(\boldsymbol{x}_t - \frac{\beta_t}{\sqrt{1-\overline{\alpha}_t}}\boldsymbol{\epsilon}_{\boldsymbol{\theta}^*}(\boldsymbol{x}_t, t)\right)/\sqrt{1-\beta_t} + \sqrt{\beta_t}\boldsymbol{\epsilon}, \tag{5}$$

where β_t is the noise level at step t, $\hat{\boldsymbol{x}}_{t-1}$ is the recovered image in step $t-1$, $\boldsymbol{\epsilon}$ is sampled from $\mathcal{N}(\mathbf{0}, \boldsymbol{I})$. DDIM proposes to speed up the denoising process by skipping certain intermediate steps. Recent work suggests that DDPM may also benefit from a similar approach (Nichol & Dhariwal, 2021). Score SDEs (Song et al., 2021a) give a score function view of DDPM and further lead to the derivations of DDPM++ (VPSDE) and EDM (Karras et al., 2022). In this diffusion process, the noise terms $\boldsymbol{\epsilon}$ in Equation (2) and Equation (5) represent the key stochastic elements that control the randomness of the process. More discussion of stochastic elements is provided in Appendix C.1.

Diffusion-based purification (DBP). DBP uses diffusion models to remove adversarial perturbation from images. Instead of using a complete diffusion process between the clean image and pure Gaussian noise (between $t = 0$ and $t = T$), they first diffuse $\boldsymbol{x}_0$ to a predefined timestep $t = t^*(t^* < T)$ via Equation (2), and recover the image $\hat{\boldsymbol{x}}_0$ via the reverse diffusion process in Equation (5).

4 STOCHASTICITY-DRIVEN ROBUSTNESS OF DBP

4.1 STOCHASTICITY AS THE MAIN FACTOR OF DBP ROBUSTNESS

As discussed in Section 2, previous studies primarily attribute the robustness of DBP to the forward diffusion process, which introduces Gaussian noise to inputs, thereby narrowing the distribution gap between the adversarial images and clean images (Nie et al., 2022; Wang et al., 2022). As a result, adversarial perturbation can be "washed out" by Gaussian noise. However, it has also been observed that the robustness of DiffPure diminishes when switching from Stochastic Differential Equation (SDE) sampling to Ordinary Differential Equation (ODE) (Nie et al., 2022), which introduce less randomness. This reduction in robustness cannot be fully explained by the "wash out" effect of Gaussian noise, indicating that stochasticity plays a role in the robustness of DBP.

To assess whether stochasticity has a significant influence on DBP robustness, we implement DDPM and DDIM within the DiffPure framework (Nie et al., 2022), resulting in $\mathbf{DP_{DDPM}}$ and $\mathbf{DP_{DDIM}}$, respectively. Note that the original implementation of DiffPure adopts a DDPM discretization form of DDPM++ (VPSDE), which has minimal differences compared to DDPM. Therefore, the main difference between DiffPure and our DP_{DDPM} is that DiffPure employs a larger UNet. DDIM, which builds upon DDPM, introduces a deterministic ODE-based reverse process. $\mathbf{DP_{DDPM}}$ introduces Gaussian noise in both the forward and reverse processes, making the entire process stochastic. In contrast, $\mathbf{DP_{DDIM}}$ introduces Gaussian noise only in the forward process, and the reverse process is deterministic. The clean and robust accuracy of the two models on CIFAR-10 (Krizhevsky et al., 2009) under white-box Projected Gradient Descent (PGD) (Madry et al., 2018)+Expectation over Transformation (EoT) (Athalye et al., 2018b) attack (as detailed in Section 6.1) are presented in Figure 2 (*Clean* and *White*). Although DP_{DDPM} achieves higher clean accuracy, it exhibits lower robust accuracy under adaptive white-box attacks, consistent with the observation by Nie et al. (2022). However, this comparison is insufficient to reveal the full role of stochasticity in DBP robustness, as the forward process of both DDPM and DDIM are stochastic.

To isolate the impact of stochasticity, we introduce a novel attack setting called the **Deterministic White-Box** (DW-box) setting. In this setting, the attacker has complete knowledge of not only the model parameters but also the specific values of the stochastic elements sampled during evaluation, effectively making the diffusion process deterministic from the attacker's perspective. This setting could be realistic if the attacker is aware of the seed or initial random state used for pseudo-random number generation in the model. Specifically, we define three levels of attacker knowledge for our evaluations: (1) Conventional **White-box** setting, where the attacker has access to the model parameters but not the stochastic elements; (2) $\mathbf{DW_{Fwd}}$**-box/**$\mathbf{DW_{Rev}}$**-box** setting, where the attacker knows the stochastic elements in the forward/reverse process, in addition to the model parameters; (3) $\mathbf{DW_{Both}}$**-box** setting, where the attacker has full knowledge of the model parameters and all the stochastic elements in both the forward and reverse processes. Details of these settings are provided in Appendix C.2.

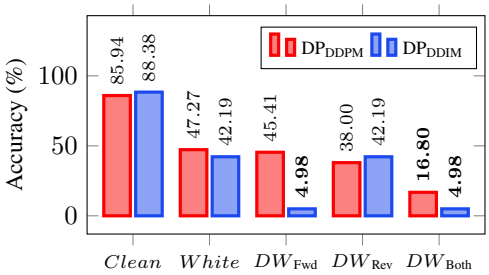

Figure 2: DP_{DDPM} and DP_{DDIM} robust accuracy under different attack settings on CIFAR-10. Both models lose most of their robustness only when the attacker knows all stochastic elements (highlighted in bold: DW_{Both}-box for DP_{DDPM}/DP_{DDIM} and DW_{Fwd}-box for DP_{DDIM}).

We evaluated adversarial robustness on CIFAR-10 using ℓ_∞ attacks (see Section 6.1). Traditional theories emphasize forward diffusion process as the primary defense mechanism, suggesting that both DP_{DDPM} and DP_{DDIM} should behave similarly under the DW_{Fwd}-box setting. However, if stochasticity throughout the diffusion process is crucial, DP_{DDIM}, which becomes deterministic under the DW_{Fwd}-box setting, should experience a notable reduction in robustness, similar to DP_{DDPM} under the DW_{Both}-box setting. As shown in Figure 2, under the DW_{Fwd}-box setting, DP_{DDPM} maintains a significant portion of its robustness, whereas DP_{DDIM} loses almost all of its resistance to adversarial attacks. Furthermore, DP_{DDPM} exhibits a substantial drop in robustness only when the attacker has full access to both the forward and reverse stochastic elements, as seen in the DW_{Both}-box setting. This suggests that stochasticity across both the forward and reverse diffusion processes plays a critical role in maintaining robustness, challenging the conventional focus on forward diffusion process alone.

Table 1: Evaluation of state-of-the-art DBP methods, EoT significantly influences the evaluation accuracy (%) of model robustness.

Metric	DiffPure	GDMP (MSE)	DP_{DDPM}	DP_{DDIM}
Clean	89.26	91.80	85.94	88.38
PGD20+EoT1	69.04	53.13	60.25	54.59
PGD20+EoT10	55.96	40.97	47.27	42.19

Our findings suggest that DBP models primarily rely on stochasticity to resist adversarial attacks, rather than depending on the forward diffusion process to mitigate adversarial perturbations. Additionally, this work reveals that DBP itself lacks the ability to *effectively purify adversarial perturbations*.

4.2 Explaining Stochasticity-Driven Robustness

To elucidate the robustness of DBP models, particularly under EoT evaluations, we analyze the performance of several DBP models—DiffPure, GDMP, DP_{DDPM}, and DP_{DDIM}—under white-box

attacks, both with and without EoT iterations (denoted as EoT10 and EoT1, respectively). The results shown in Table 1 indicate that these DBP models remain robust under white-box attacks, with EoT evaluations leading to moderate reductions in robustness. A more detailed discussion of EoT steps is provided in Appendix A.

To gain further insights, we visualize the attack trajectories using t-SNE, projecting them onto a *xy*-plane with loss values represented along the *z*-axis. We compare trajectories for three types of attacks: white-box without EoT (White-box), white-box with EoT (White-box-EoT), and Deterministic White-box (DW-box). As shown in Figure 1, the trajectories exhibit high variance across all settings, reflecting the stochastic nature of DBP models. Specifically, DW-box attacks lead to a significant increase in loss values, while white-box attacks, even with EoT, cause only moderate increases. This suggests that *stochasticity prevents attackers from finding the optimal attack direction*. Due to the high variance in the attack gradients, even if the EoT direction provides an accurate estimate of the mean gradient direction, it may not perfectly align with the most effective direction for the DW-box attack. This leads to a reduction in attack performance. Additional evidence is provided in Appendix B.

Further analysis of the loss landscape, presented in Figure 3, highlights key differences between White-box-EoT and Deterministic White-box attacks. The trajectory of the White-box-EoT attack diverges from that of the Deterministic White-box attack, resulting in a flatter loss landscape along the White-box-EoT path. This behavior suggests that White-box-EoT attacks struggle to find the most effective direction due to the stochastic nature of DBP models. In contrast, the Deterministic White-box attack causes a sharp increase in loss. This indicates that when stochasticity is removed, the model becomes more vulnerable to adversarial perturbations. These findings differ from models trained using AT, where the loss landscape tends to remain flat and resistant across adversarial directions (Shafahi et al., 2019).

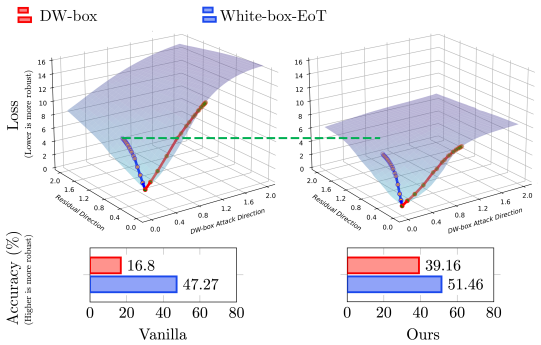

Figure 3: Visualisation of attack trajectories for White-box-EoT attacks and DW-box attacks on the loss landscape. The loss landscape is steep in the direction of the DW-box attack. The plot is based on the first 128 images of CIFAR-10.

In conclusion, we propose that, rather than *having a flat loss landscape*, DBP models rely on stochasticity to *evade the most effective attack directions*. Note that while certified defense methods like random smoothing also incorporate stochasticity (Xiao et al., 2022; Carlini et al., 2022), their mechanisms and implications differ from those of DBP methods, as discussed in Appendix D.

5 Towards Improving the Purification Capability of DBP Models

Based on the analysis in Section 4, although the stochasticity-driven robustness of DBP does not depend on the flatness of the loss landscape, flattening the landscape can still benefit DBP robustness due to the non-trivial loss increment along the EoT direction. To achieve a flat loss landscape, it is necessary to introduce adversarial samples to the training of DBP models and minimize the loss on them. From the perspective of adversarial purification, this involves improving the diffusion model's ability to purify adversarial perturbations.

To address this, we propose **Adversarial Denoising Diffusion Training (ADDT)**, a method that incorporates adversarial perturbations into the training of the diffusion model in DBP. ADDT follows an iterative two-step process: (1) **Classifier-Guided Perturbation Optimization (CGPO)**, which generates adversarial perturbations by maximizing the classification error of a pre-trained classifier; (2) **Diffusion Model Training**, which updates the diffusion model using these perturbations to improve its capability of adversarial purification.

Integrating adversarial perturbations into diffusion training poses a challenge due to the Gaussian noise assumption inherent in diffusion models. To address this, we introduce **Rank-Based Gaussian Mapping (RBGM)**, a technique designed to transform adversarial perturbations into a form that

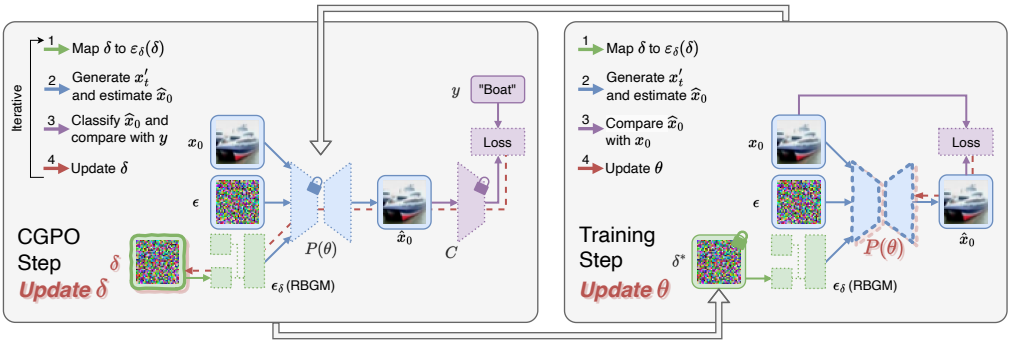

Figure 4: Overview of Adversarial Denoising Diffusion Training (ADDT). ADDT alternates between a CGPO step (left grey box) to refine the perturbations with a frozen diffusion model and classifier, and a training step (right grey box) to update the diffusion model with the refined perturbation. Throughout the process, RBGM is used to make the perturbation more "Gaussian-like".

aligns with the Gaussian noise assumption. RBGM makes the perturbations more "Gaussian-like", thus facilitating their integration into the diffusion training process.

An overview of ADDT is provided in Figure 4, with pseudocode available in Appendix G. The following subsections detail the components of ADDT.

5.1 Adversarial Denoising Diffusion Training

Classifier-Guided Perturbation Optimization (CGPO) step. In this step, we aim to refine adversarial perturbations $\boldsymbol{\delta}$ in a way that maximizes the classification error of a pre-trained classifier C. The process starts by reconstructing a clean image $\hat{\boldsymbol{x}}_0$ from the perturbed input $\boldsymbol{x}'_t$ using the diffusion model $\boldsymbol{P}$. The perturbed input $\boldsymbol{x}'_t$ is generated from the original image $\boldsymbol{x}_0$, Gaussian noise $\boldsymbol{\epsilon}$, and the RBGM-mapped adversarial perturbation $\boldsymbol{\epsilon}_{\boldsymbol{\delta}}(\boldsymbol{\delta})$, which will be detailed in Section 5.2. $\boldsymbol{P}(\boldsymbol{\theta}, \boldsymbol{x}'_t, t)$ denotes a one-step diffusion process, which takes the noisy input $\boldsymbol{x}'_t$ and time step t and reconstructs the image $\hat{\boldsymbol{x}}_0$, following the formulation in Equation (4). The classifier C is then applied to this reconstructed image $\hat{\boldsymbol{x}}_0$ to predict a label. The optimization objective is to maximize the discrepancy between the predicted label and the ground-truth label y. This can be formulated as:

$$\boldsymbol{\delta}^* = \arg\max_{\boldsymbol{\delta}} \mathbb{E}_{\boldsymbol{x}_0, t, \boldsymbol{\epsilon}} \left[L\left(C\left(\boldsymbol{P}\left(\boldsymbol{\theta}, \boldsymbol{x}'_t(\boldsymbol{x}_0, \boldsymbol{\epsilon}, \boldsymbol{\epsilon}_{\boldsymbol{\delta}}(\boldsymbol{\delta})), t \right) \right), y \right) \right], \tag{6}$$

where $L(\cdot, y)$ denotes the loss function measuring the discrepancy between the classifier's prediction and the ground-truth label y. The pre-trained classifier C provides semantic guidance and need not be identical to the protected classifier, as detailed in Section 6.2. To optimize $\boldsymbol{\delta}$, we employ the PGD attack (Madry et al., 2018). Given that RBGM is non-differentiable, we adopt the Backward Pass Differentiable Approximation (BPDA) approach (Athalye et al., 2018a), which utilizes RBGM during forward propagation while bypassing it during back-propagation.

Diffusion Model Training step. The goal of this step is to update the diffusion model parameters to accurately recover the original image $\boldsymbol{x}_0$ from a perturbed version $\boldsymbol{x}'_t$. As illustrated on the right side of Figure 4, the model aims to remove both the Gaussian noise and the adversarial perturbations, effectively denoising the input. The optimization objective is defined as:

$$\boldsymbol{\theta}^* = \arg\min_{\boldsymbol{\theta}} \mathbb{E}_{\boldsymbol{x}_0, t, \boldsymbol{\epsilon}} \left[\frac{\sqrt{\overline{\alpha}_t}}{\sqrt{1 - \overline{\alpha}_t}} \left\| \boldsymbol{x}_0 - \boldsymbol{P}(\boldsymbol{\theta}, \boldsymbol{x}'_t(\boldsymbol{x}_0, \boldsymbol{\epsilon}, \boldsymbol{\epsilon}_{\boldsymbol{\delta}}(\boldsymbol{\delta})), t) \right\|_2^2 \right], \tag{7}$$

where the scaling factor $\sqrt{\overline{\alpha}_t}/\sqrt{1 - \overline{\alpha}_t}$ ensures consistency with the standard formulation of DDPM/DDIM loss. This factor reflects the expected squared error between the noise introduced to the input and the noise removed by the diffusion model during denoising.

5.2 Rank-Based Gaussian Mapping

Traditional diffusion models operate under the premise that input images are corrupted by independent Gaussian noise $\boldsymbol{\epsilon}$. To ensure that perturbations maintain Gaussian-like characteristics while capturing adversarial features, we introduce the Rank-Based Gaussian Mapping (RBGM), denoted as $\boldsymbol{\epsilon}_{\boldsymbol{\delta}}(\boldsymbol{\delta})$

and illustrated in Figure 5. The key idea is to preserve the rank ordering of the elements in $\boldsymbol{\delta}$ but replace their actual values with those from a standard Gaussian distribution. Specifically, we sample a Gaussian tensor $\boldsymbol{\epsilon}_s$ of the same dimensions as $\boldsymbol{\delta}$. We then sort the elements of both $\boldsymbol{\delta}$ and $\boldsymbol{\epsilon}_s$ respectively in ascending order. By mapping the sorted elements of $\boldsymbol{\delta}$ to t he corresponding elements of $\boldsymbol{\epsilon}_s$, we obtain $\boldsymbol{\epsilon}_{\boldsymbol{\delta}}(\boldsymbol{\delta})$, which approximates Gaussian-distributed but retains the structural information of $\boldsymbol{\delta}$. To further enhance the Gaussian-like characteristics of the perturbations, we combine the RBGM-mapped noise with additional random Gaussian noise. This results in the adversarial input $\boldsymbol{x}_t'$, defined as follows:

$$\boldsymbol{x}_t'(\boldsymbol{x}_0, \boldsymbol{\epsilon}, \boldsymbol{\epsilon}_{\boldsymbol{\delta}}(\boldsymbol{\delta})) = \sqrt{\overline{\alpha}_t}\boldsymbol{x}_0 + \sqrt{1-\lambda_t^2}\sqrt{1-\overline{\alpha}_t}\boldsymbol{\epsilon} + \lambda_t\sqrt{1-\overline{\alpha}_t}\boldsymbol{\epsilon}_{\boldsymbol{\delta}}(\boldsymbol{\delta}), \tag{8}$$

where λ_t modulates the level of adversarial perturbation. This ensures that the overall noise remains largely independent of $\boldsymbol{x}_0$ and that the perturbations do not overwhelm the denoising model's learning capabilities. We determine λ_t using the following formulation:

$$\lambda_t = \texttt{clip}(\gamma_t \lambda_{unit}, \lambda_{min}, \lambda_{max}), \quad \gamma_t = \sqrt{\overline{\alpha}_t}/\sqrt{1-\overline{\alpha}_t}, \tag{9}$$

where the $\texttt{clip}$ function limits λ_t between λ_{min} and λ_{max}. Additional details and discussions about RBGM can be found in Appendix K.

6 Experiments and Discussions

6.1 Experiment Setups

Classifier. We train a WideResNet-28-10 for 200 epochs following the methods in Yoon et al. (2021); Wang et al. (2022), achieving 95.12% accuracy on CIFAR-10 and 76.66% on CIFAR-100 dataset.

DBP timestep. For the diffusion forward process, we adopt the same timestep settings as DiffPure (Nie et al., 2022). In continuous-time models, such as the VPSDE (DDPM++) variant, with the forward time parameter $0 \leq t \leq 1$, we set $t^* = 0.1$, which strikes a balance between noise introduction and computational efficiency. For discrete-time models, such as DDPM and DDIM, where $t = 0, 1, ..., T$, we similarly set the timestep to $t^* = 0.1 \times T$. Additional settings and results on DP_{EDM} are provided in Appendix I.

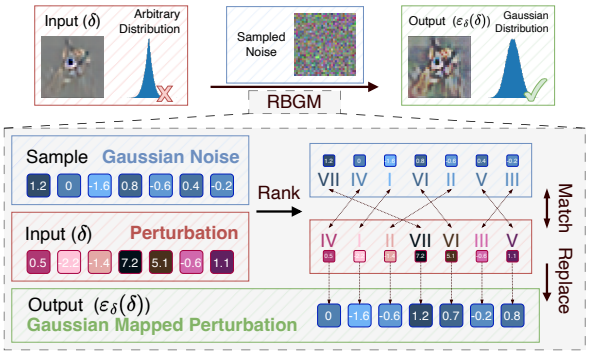

Figure 5: Rank-Based Gaussian Mapping. RBGM trims the input to follow Gaussian distribution. It samples a Gaussian noise and then replaces elements in the input with corresponding values from the noise, based on matching ranks.

Robustness evaluation. We employ PGD20+EoT10 (Athalye et al., 2018b) attack for assessing model robustness. For ℓ_∞-norm attacks, we set the step size $\alpha = 2/255$ and the maximum perturbation $\epsilon = 8/255$, while for ℓ_2-norm attacks, we use $\alpha = 0.1$ and $\epsilon = 0.5$. Due to the high computational cost of EoT attacks, we evaluate our models on the first 1024 images for CIFAR-10 and CIFAR-100 datasets. For comprehensive evaluation settings, including an analysis of AutoAttack (Croce & Hein, 2020) performance on DBP models, refer to Appendix E.

Table 2: Clean and robust accuracy (%) on CIFAR-10, obtained by different classifiers. ADDT (WRN-28-10 guidance) improves robustness in protecting different subsequent classifiers. (*: the classifier used in ADDT fine-tuning).

DBP method	Classifier	Vanilla			ADDT		
		Clean	l_∞	l_2	*Clean*	l_∞	l_2
DP_{DDPM}	VGG-16 (Simonyan & Zisserman, 2014)	84.77	41.99	66.89	85.06	**46.09**	**67.87**
	ResNet-50 (He et al., 2016)	83.11	44.04	67.58	83.84	**48.14**	**67.87**
	WRN-28-10* (Zagoruyko & Komodakis, 2016)	85.94	47.27	69.34	85.64	**51.46**	**70.12**
	WRN-70-16 (Zagoruyko & Komodakis, 2016)	88.43	48.93	70.31	87.84	**52.54**	**70.70**
	ViT-B (Dosovitskiy et al., 2020)	85.45	45.61	69.53	85.25	**48.63**	**69.92**
DP_{DDIM}	VGG-16 (Simonyan & Zisserman, 2014)	87.16	29.00	61.82	87.55	**35.06**	**66.11**
	ResNet-50 (He et al., 2016)	86.04	31.74	62.11	86.57	**38.77**	**65.82**
	WRN-28-10* (Zagoruyko & Komodakis, 2016)	88.96	43.16	67.58	88.18	**47.85**	**70.61**
	WRN-70-16 (Zagoruyko & Komodakis, 2016)	84.40	39.16	68.36	84.96	**47.66**	**69.14**
	ViT-B (Dosovitskiy et al., 2020)	88.77	34.38	65.72	88.48	**41.02**	**68.65**
DP_{EDM}	WRN-28-10* (Zagoruyko & Komodakis, 2016)	86.43	62.50	76.86	86.33	**66.41**	**79.16**
	WRN-70-16 (Zagoruyko & Komodakis, 2016)	86.62	65.62	76.46	86.43	**69.63**	**78.91**

Table 3: Clean and robust accuracy (%) on CIFAR-10 obtained by different DBP methods. All methods show consistent improvement fine-tuned with ADDT.

Diffusion model	DBP method	*Clean*	ℓ_∞	ℓ_2
-	-	95.12	0.00	1.46
DDIM	DP_{DDIM}	88.38	42.19	70.02
	DP_{DDIM}+ADDT	88.77	**46.48**	**71.19**
DDPM	GDMP (No Guided) (Wang et al., 2022)	91.41	40.82	69.63
	GDMP (MSE) (Wang et al., 2022)	91.80	40.97	70.02
	GDMP (SSIM) (Wang et al., 2022)	92.19	38.18	68.95
	DP_{DDPM}	85.94	47.27	69.34
	DP_{DDPM}+ADDT	85.64	**51.46**	**70.12**
DDPM++	COUP (Zhang et al., 2024)	90.33	50.78	71.19
	DiffPure	89.26	55.96	75.78
	DiffPure+ADDT	89.94	**62.11**	**76.66**
EDM	DP_{EDM} (Appendix I)	86.43	62.50	76.86
	DP_{EDM}+ADDT (Appendix I)	86.33	**66.41**	**79.16**

Table 4: Clean and robust accuracy (%) on DP_{DDPM}. ADDT improve robustness across different NFEs, especially at lower NFEs (*: default DDPM generation setting; -: classifier only).

Dataset	NFEs	Vanilla *Clean*	Vanilla l_∞	Vanilla l_2	ADDT *Clean*	ADDT l_∞	ADDT l_2
CIFAR-10	-	95.12	0.00	1.46	95.12	0.00	1.46
	5	49.51	21.78	36.13	59.96	**30.27**	**41.99**
	10	73.34	36.72	55.47	78.91	**43.07**	**62.97**
	20	81.45	45.21	65.23	83.89	**48.44**	**69.82**
	50	85.54	46.78	68.85	85.45	**50.20**	**69.04**
	100*	85.94	47.27	69.34	85.64	**51.46**	**70.12**
CIFAR-100	-	76.66	0.00	2.44	76.66	0.00	2.44
	5	17.29	3.71	9.28	21.78	**6.25**	**13.77**
	10	34.08	10.55	19.24	40.62	**14.55**	**27.25**
	20	48.05	17.68	30.66	53.32	**18.65**	**36.13**
	50	55.57	20.02	37.70	59.47	**22.75**	**40.72**
	100*	57.52	20.41	37.89	59.18	**23.73**	**41.70**

ADDT. ADDT fine-tuning is guided by the pre-trained WideResNet-28-10 classifier. For the CIFAR-10 dataset, we utilize the pre-trained exponential moving average (EMA) diffusion model developed by Ho et al. (2020) (converted to Huggingface Diffusers format by Fang et al. (2023)). For the CIFAR-100 dataset, we fine-tune this CIFAR-10 diffusion model over 100 epochs. In CGPO, we set the hyperparameters to $\lambda_{unit} = 0.03$, $\lambda_{min} = 0$, and $\lambda_{max} = 0.3$, and iteratively refine the perturbation δ for 5 steps. Additional details regarding computational cost are provided in Appendix O.

6.2 Defense Performance Under Different Conditions

Performance across different DBP models. We assess the effectiveness of ADDT by applying it to various diffusion models and incorporating DiffPure-style DBP with the refined models. We then compare the clean and robust accuracies of our approach, the baseline, and other DBP models, as presented in Table 3. The results demonstrate that ADDT consistently improves model robustness while maintaining competitive clean accuracy.

Performance across different downstream classifiers. We evaluate the cross-model protection capabilities of ADDT by applying the diffusion model, specifically ADDT fine-tuned with WRN-28-10 guidance, to protect various classifiers. The results in Table 2 show that these diffusion models are effective in protecting classifiers with diverse architectures. Notably, using a DP_{EDM} with WRN-28-10 Guidance training, we achieve 69.63% l_∞ robust accuracy on a WRN-70-16 classifier. This characteristic of not requiring classifier-specific fine-tuning underscores the feasibility of ADDT.

Table 5: Clean and robust accuracy (%) on CIFAR-10 fine-tuned with different training samples. (None: no fine-tuning)

DBP method	Training samples	Clean	l_∞	l_2
DP_{DDPM}	None	85.94	47.27	69.34
	Clean	85.25	47.27	68.26
	MSE-guided	86.91	46.97	**70.80**
	CGPO	85.64	**51.46**	70.12
DP_{DDIM}	None	88.96	43.16	67.58
	Clean	88.87	41.41	67.19
	MSE-guided	89.36	40.92	67.68
	CGPO	88.18	**47.85**	**70.61**

Performance under acceleration. Speeding up the diffusion process by omitting intermediate steps has become a common practice in diffusion models (Song et al., 2020; Nichol & Dhariwal, 2021). In this context, we evaluate the robustness of accelerated DBP models. To quantify computational cost, we utilize the number of Neural Function Evaluations (NFEs), which reflects the number of evaluation steps executed during the DBP backtracking process. For our experiments, we set $t^* = 0.1 \times T$ and accelerate the process by excluding intermediate time steps. For example, with 5 NFEs, the time steps for the DBP reverse process would be $t = [100, 80, 60, 40, 20, 0]$. The results in Table 4 validate the effectiveness of ADDT in improving the robustness of accelerated DP_{DDPM} models. Note that the performance of DP_{DDPM} varies significantly between different values of NFEs. This may be explained by the fact that DDPM introduces stochasticity (Gaussian noise) at each reverse step; with fewer reverse steps, its stochasticity reduces. Additionally, the generation capability of DDPM is sensitive to skipping of intermediate steps. We also conducted an evaluation of DP_{DDIM} models, as detailed in Appendix H.

6.3 Ablation Study and Analysis

RBGM. We compare the generative ability of diffusion models fine-tuned from the same pre-trained

models, using two different perturbations: RBGM-mapped perturbations and ℓ_∞ perturbations. To quantify generation quality, we compare Fréchet Inception Distance (FID) scores (Heusel et al., 2017), as presented in Table 6. The results demonstrate that diffusion models fine-tuned with RBGM-mapped perturbations maintain generation quality comparable to the vanilla diffusion model, while models directly fine-tuned with l_∞ perturbations without RBGM show degraded performance. We also observe that training with RBGM-mapped perturbations generalized better to different attacks. Experimental details and additional tests are presented in Appendix L.

Table 6: FID score of DDPM for CIFAR-10 fine-tuned to different perturbations (the lower the better). Fine-tuning with RBGM-mapped perturbations yields lower FID scores than l_∞ perturbations (without RBGM).

	Vanilla	Clean Fine-tuning	ADDT	ADDT w/o RBGM
FID	3.196	3.500	5.190	13.608

CGPO. We analyze the effect of fine-tuning using different training samples in Table 5. Specifically, we compare the performance of samples generated with classifier guidance in the CGPO step, referred to as "CGPO", against those generated with Mean Squared Error (MSE) loss, noted as "MSE-guided". The evaluation results are presented for DDPM with 100 NFEs and DDIM with 10 NFEs. The results demonstrate that samples generated by CGPO significantly outperform MSE-guided samples in enhancing DBP robustness.

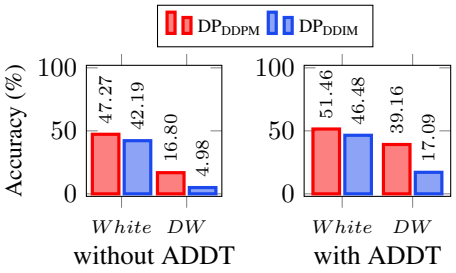

Figure 6: Revisiting robustness under Deterministic White-box setting. ADDT improves robustness under both White-box and Deterministic White-box setting, implying that ADDT strengthens the models' ability to purify adversarial inputs.

Revisiting DBP robustness. We re-examine robustness under the Deterministic White-box setting by comparing the performance of diffusion models with and without ADDT fine-tuning, as shown in Figure 6. The fine-tuned models show significantly higher robust accuracy under the DW-box setting, indicating improved non-stochasticity-based robustness brought by ADDT. Further experiments across different models and NFEs in Appendix M confirm these robustness improvements. We also compare the loss landscapes of ADDT fine-tuned models and vanilla diffusion models, as shown in Figure 3. This comparison shows that our method effectively smooths the loss landscape of DBP models and enhance its ability to purify adversarial perturbations.

Evaluation with stronger PGD+EoT attacks. To balance computational cost and attack strength, we primarily employ the PGD20+EoT10 configuration in our evaluations. To further validate the efficacy of ADDT under stronger attack settings, we assess its performance using the more challenging PGD200+EoT20 setup. The results presented in Table 7 and Table 9 show that under these intensified attacks, ADDT's robust accuracy experiences a moderate 5% drop compared to the PGD20+EoT10 setting. Nevertheless, across various configurations and datasets, ADDT consistently outperforms the baseline in terms of robust accuracy.

6.4 Scaling to More Complex and High-Dimensional Data

To evaluate the scalability of DBP and ADDT on more complex and high-dimensional datasets, we extend our experiments to include Tiny-ImageNet (Le & Yang, 2015) and ImageNet-1k (Deng et al., 2009). For Tiny-ImageNet, we trained the diffusion model from scratch for 200 epochs, followed by 50 epochs of fine-tuning with ADDT, using a pretrained WRN-28-10 classifier as guidance. For ImageNet-1k, the diffusion model was trained from scratch for 12 epochs, followed by 8 epochs of fine-tuning with ADDT, with guidance from a pretrained ResNet-101 classifier.

Table 7: Robust accuracy (%) on CIFAR-10 under more PGD and EoT iterations.

DBP method	PGD200+EoT20		PGD20+EoT10	
	Vanilla (ℓ_∞)	ADDT (ℓ_∞)	Vanilla (ℓ_∞)	ADDT (ℓ_∞)
DP$_{\text{DDPM}}$	41.02	**46.19**	47.27	**51.46**
DP$_{\text{DDIM}}$	36.23	**41.11**	43.16	**47.85**
DiffPure	48.93	**55.76**	55.96	**62.11**

As shown in Table 8 and Table 9, ADDT improves the robustness of DBP on these complex datasets. However, the additional robustness provided by ADDT appears somewhat limited. This suggests that for ADDT to scale more effectively, a sufficiently large model capacity and a substantial amount of data may be necessary. This is further supported by the results in Table 3, where the larger

Table 8: Clean and robust accuracy (%) on Tiny-ImageNet with WRN-28-10 classifier. ADDT improves DBP robustness on Tiny-ImageNet (-: classifier only).

DBP method	Vanilla			ADDT		
	Clean	l_∞	l_2	Clean	l_∞	l_2
-	71.37	0.00	0.00	-	-	-
DP_{DDPM}	57.13	11.82	46.68	56.15	**13.57**	**48.54**
DP_{DDIM}	60.35	4.79	39.75	60.45	**5.86**	**40.82**
DP_{EDM}	57.03	19.14	46.00	56.45	**20.61**	**47.95**

Table 9: Clean and robust accuracy (%) on ImageNet-1k with ResNet-101 classifier. All experiments are conducted under l_∞ perturbation bound of $\epsilon = 4/255$.

Metric	Vanilla	ADDT
Clean	80.31	80.20
PGD20+EoT10	46.92	**48.02**
PGD200+EoT20	35.31	**35.83**

DiffPure+ADDT model exhibits greater robustness compared to the smaller DP_{DDPM}+ADDT model, aligning with findings from traditional AT (Wang et al., 2023; Huang et al., 2023).

It is also important to note that scaling to high-resolution images poses a significant challenge for attackers, as executing strong EoT attacks on high-resolution images is computationally intensive. For instance, our evaluation with PGD200+EoT20 on 224×224 images at a resolution of 1024 takes approximately 7 days of computation on 8 NVIDIA RTX 4090 GPUs.

6.5 Discussions on Improving Stochasticity-based DBP Robustness

As analyzed in Section 4.2, the DBP robustness can be primarily attributed to the high variance of the stochastic attack gradients. We argue that *increasing the variance of attack gradients* can improve the stochasticity-based robustness of DBP models by reducing the effectiveness of EoT attacks. Specifically, on the one hand, higher variance means higher errors in the estimation of the expected attack gradient direction with a fixed number of samples, and to reduce the error, more EoT steps are required. On the other hand, higher variance also suggests that the expected deviation of the DW-box attack gradient (which suggests the most effective attack direction) deviates more from the EoT attack gradient, even if the estimation of the mean attack gradient is accurate. As discussed in Section 4.2, such deviation leads to lower increase in classification loss for one attack step, suggesting that a successful attack may not be achieved or require more PGD steps.

To increase the variance of attack gradients, an intuitive approach is to introduce more stochasticity. As an initial experiment, we augment the DBP framework's stochasticity by integrating a *Corrector sampler*. Specifically, Song et al. (2021b) develop a Predictor-Corrector (PC) sampler framework. While standard VPSDE (DDPM++) implementations typically use only the predictor component, we add a Corrector sampler to increase stochasticity in the reverse diffusion process, thereby boosting the overall variance of attack gradients. As detailed in Appendix J, our preliminary results indicate that this modification improves the robustness of DBP models against adaptive White-box attacks. However, there is a trade-off: the model's clean accuracy decreases slightly. These observations align with the findings of Nie et al. (2022), where randomizing the diffusion timesteps also leads to robustness improvements at the cost of clean accuracy, as well as with prior research on stochastic preprocessing defenses (Gao et al., 2022).

7 Conclusion

This study offers a new perspective on the robustness of Diffusion-Based Purification (DBP), emphasizing the crucial role of stochasticity and challenging the traditional view that robustness is mainly derived from minimizing the distribution gap through the forward diffusion process. We introduce a Deterministic white-box (DW-box) attack setting and show that DBP models are based on stochastic elements to evade effective attack directions and lack the ability to purify adversarial perturbations, demonstrating distinct properties compared to models trained with Adversarial Training. To further enhance the robustness of DBP models, we develop Adversarial Denoising Diffusion Training (ADDT) and Rank-Based Gaussian Mapping (RBGM). ADDT integrates adversarial perturbations into the training process, while RBGM trims perturbations to more closely resemble Gaussian distributions. Experiments across various diffusion methods, attack settings, and datasets suggest the effectiveness of ADDT. In summary, this study highlights the decoupling of stochasticity-based and purification-based robustness of DBP models for deeper analysis, and suggests combining them for better robustness in practice.

ACKNOWLEDGEMENTS

This work is supported in part by National Natural Science Foundation of China (NSFC) under Grant No.62376292, U21A20470, Guangdong Provincial General Fund No. 2024A1515010208.

We would like to express our sincere gratitude to **Hongjun Wang**, **Zhaoyu Chen**, **Huanran Chen**, **Ruoxin Chen** and **Conghan Yue** for their invaluable discussions, which greatly contributed to the development of this work.

REFERENCES

Anish Athalye, Nicholas Carlini, and David Wagner. Obfuscated gradients give a false sense of security: Circumventing defenses to adversarial examples. In *International conference on machine learning*, pp. 274–283. PMLR, 2018a.

Anish Athalye, Logan Engstrom, Andrew Ilyas, and Kevin Kwok. Synthesizing robust adversarial examples. In *International conference on machine learning*, pp. 284–293. PMLR, 2018b.

Nicholas Carlini, Florian Tramer, Krishnamurthy Dj Dvijotham, Leslie Rice, Mingjie Sun, and J Zico Kolter. (certified!!) adversarial robustness for free! In *The Eleventh International Conference on Learning Representations*, 2022.

Huanran Chen, Yinpeng Dong, Zhengyi Wang, Xiao Yang, Chengqi Duan, Hang Su, and Jun Zhu. Robust classification via a single diffusion model. *arXiv preprint arXiv:2305.15241*, 2023.

Tianqi Chen, Bing Xu, Chiyuan Zhang, and Carlos Guestrin. Training deep nets with sublinear memory cost. *arXiv preprint arXiv:1604.06174*, 2016.

Jeremy Cohen, Elan Rosenfeld, and Zico Kolter. Certified adversarial robustness via randomized smoothing. In *international conference on machine learning*, pp. 1310–1320. PMLR, 2019.

Francesco Croce and Matthias Hein. Reliable evaluation of adversarial robustness with an ensemble of diverse parameter-free attacks. In *International conference on machine learning*, pp. 2206–2216. PMLR, 2020.

Francesco Croce, Maksym Andriushchenko, Vikash Sehwag, Edoardo Debenedetti, Nicolas Flammarion, Mung Chiang, Prateek Mittal, and Matthias Hein. Robustbench: a standardized adversarial robustness benchmark. *arXiv preprint arXiv:2010.09670*, 2020.

Jia Deng, Wei Dong, Richard Socher, Li-Jia Li, Kai Li, and Li Fei-Fei. Imagenet: A large-scale hierarchical image database. In *2009 IEEE conference on computer vision and pattern recognition*, pp. 248–255. Ieee, 2009.

Alexey Dosovitskiy, Lucas Beyer, Alexander Kolesnikov, Dirk Weissenborn, Xiaohua Zhai, Thomas Unterthiner, Mostafa Dehghani, Matthias Minderer, Georg Heigold, Sylvain Gelly, et al. An image is worth 16x16 words: Transformers for image recognition at scale. *arXiv preprint arXiv:2010.11929*, 2020.

Gongfan Fang, Xinyin Ma, and Xinchao Wang. Structural pruning for diffusion models. *arXiv preprint arXiv:2305.10924*, 2023.

Yue Gao, Ilia Shumailov, Kassem Fawaz, and Nicolas Papernot. On the limitations of stochastic pre-processing defenses. *Advances in Neural Information Processing Systems*, 35:24280–24294, 2022.

Ian J. Goodfellow, Jonathon Shlens, and Christian Szegedy. Explaining and harnessing adversarial examples. In Yoshua Bengio and Yann LeCun (eds.), *3rd International Conference on Learning Representations, ICLR 2015, San Diego, CA, USA, May 7-9, 2015, Conference Track Proceedings*, 2015. URL `http://arxiv.org/abs/1412.6572`.

Sven Gowal, Chongli Qin, Jonathan Uesato, Timothy A. Mann, and Pushmeet Kohli. Uncovering the limits of adversarial training against norm-bounded adversarial examples. *CoRR*, abs/2010.03593, 2020. URL `https://arxiv.org/abs/2010.03593`.

Sven Gowal, Sylvestre-Alvise Rebuffi, Olivia Wiles, Florian Stimberg, Dan Andrei Calian, and Timothy A Mann. Improving robustness using generated data. *Advances in Neural Information Processing Systems*, 34:4218–4233, 2021.

Kaiming He, Xiangyu Zhang, Shaoqing Ren, and Jian Sun. Deep residual learning for image recognition. In *Proceedings of the IEEE conference on computer vision and pattern recognition*, pp. 770–778, 2016.

Martin Heusel, Hubert Ramsauer, Thomas Unterthiner, Bernhard Nessler, and Sepp Hochreiter. Gans trained by a two time-scale update rule converge to a local nash equilibrium. *Advances in neural information processing systems*, 30, 2017.

Jonathan Ho, Ajay Jain, and Pieter Abbeel. Denoising diffusion probabilistic models. *arXiv preprint arxiv:2006.11239*, 2020.

Shihua Huang, Zhichao Lu, Kalyanmoy Deb, and Vishnu Naresh Boddeti. Revisiting residual networks for adversarial robustness. In *Proceedings of the IEEE/CVF conference on computer vision and pattern recognition*, pp. 8202–8211, 2023.

Mintong Kang, Dawn Song, and Bo Li. Diffattack: Evasion attacks against diffusion-based adversarial purification. *Advances in Neural Information Processing Systems*, 36, 2024.

Tero Karras, Miika Aittala, Timo Aila, and Samuli Laine. Elucidating the design space of diffusion-based generative models. *Advances in Neural Information Processing Systems*, 35:26565–26577, 2022.

Alex Krizhevsky, Geoffrey Hinton, et al. Learning multiple layers of features from tiny images. 2009.

Ya Le and Xuan Yang. Tiny imagenet visual recognition challenge. *CS 231N*, 7(7):3, 2015.

Aleksander Madry, Aleksandar Makelov, Ludwig Schmidt, Dimitris Tsipras, and Adrian Vladu. Towards deep learning models resistant to adversarial attacks. In *6th International Conference on Learning Representations, ICLR 2018, Vancouver, BC, Canada, April 30 - May 3, 2018, Conference Track Proceedings*. OpenReview.net, 2018. URL https://openreview.net/forum?id=rJzIBfZAb.

Alexander Quinn Nichol and Prafulla Dhariwal. Improved denoising diffusion probabilistic models. In *International Conference on Machine Learning*, pp. 8162–8171. PMLR, 2021.

Weili Nie, Brandon Guo, Yujia Huang, Chaowei Xiao, Arash Vahdat, and Anima Anandkumar. Diffusion models for adversarial purification. In *International Conference on Machine Learning (ICML)*, 2022.

OpenAI. Gpt-4 technical report. *ArXiv*, abs/2303.08774, 2023. URL https://api.semanticscholar.org/CorpusID:257532815.

Alec Radford, Jong Wook Kim, Tao Xu, Greg Brockman, Christine McLeavey, and Ilya Sutskever. Robust speech recognition via large-scale weak supervision. In *International conference on machine learning*, pp. 28492–28518. PMLR, 2023.

Sylvestre-Alvise Rebuffi, Sven Gowal, Dan Andrei Calian, Florian Stimberg, Olivia Wiles, and Timothy A. Mann. Fixing data augmentation to improve adversarial robustness. *ArXiv*, abs/2103.01946, 2021. URL https://api.semanticscholar.org/CorpusID:232092181.

Pouya Samangouei, Maya Kabkab, and Rama Chellappa. Defense-gan: Protecting classifiers against adversarial attacks using generative models. *arXiv preprint arXiv:1805.06605*, 2018.

Ali Shafahi, Mahyar Najibi, Mohammad Amin Ghiasi, Zheng Xu, John Dickerson, Christoph Studer, Larry S Davis, Gavin Taylor, and Tom Goldstein. Adversarial training for free! *Advances in Neural Information Processing Systems*, 32, 2019.

Karen Simonyan and Andrew Zisserman. Very deep convolutional networks for large-scale image recognition. *arXiv preprint arXiv:1409.1556*, 2014.

Jiaming Song, Chenlin Meng, and Stefano Ermon. Denoising diffusion implicit models. *arXiv:2010.02502*, October 2020. URL https://arxiv.org/abs/2010.02502.

Yang Song, Taesup Kim, Sebastian Nowozin, Stefano Ermon, and Nate Kushman. Pixeldefend: Leveraging generative models to understand and defend against adversarial examples. In *International Conference on Learning Representations*, 2018. URL https://openreview.net/forum?id=rJUYGxbCW.

Yang Song, Jascha Sohl-Dickstein, Diederik P Kingma, Abhishek Kumar, Stefano Ermon, and Ben Poole. Score-based generative modeling through stochastic differential equations. In *International Conference on Learning Representations*, 2021a. URL https://openreview.net/forum?id=PxTIG12RRHS.

Yang Song, Jascha Sohl-Dickstein, Diederik P Kingma, Abhishek Kumar, Stefano Ermon, and Ben Poole. Score-based generative modeling through stochastic differential equations. In *International Conference on Learning Representations*, 2021b. URL https://openreview.net/forum?id=PxTIG12RRHS.

Christian Szegedy, Wojciech Zaremba, Ilya Sutskever, Joan Bruna, Dumitru Erhan, Ian J. Goodfellow, and Rob Fergus. Intriguing properties of neural networks. In Yoshua Bengio and Yann LeCun (eds.), *2nd International Conference on Learning Representations, ICLR 2014, Banff, AB, Canada, April 14-16, 2014, Conference Track Proceedings*, 2014. URL http://arxiv.org/abs/1312.6199.

Jinyi Wang, Zhaoyang Lyu, Dahua Lin, Bo Dai, and Hongfei Fu. Guided diffusion model for adversarial purification. *arXiv preprint arXiv:2205.14969*, 2022.

Zekai Wang, Tianyu Pang, Chao Du, Min Lin, Weiwei Liu, and Shuicheng Yan. Better diffusion models further improve adversarial training. In *International Conference on Machine Learning (ICML)*, 2023.

Quanlin Wu, Hang Ye, and Yuntian Gu. Guided diffusion model for adversarial purification from random noise. *arXiv preprint arXiv:2206.10875*, 2022.

Chaowei Xiao, Zhongzhu Chen, Kun Jin, Jiongxiao Wang, Weili Nie, Mingyan Liu, Anima Anandkumar, Bo Li, and Dawn Song. Densepure: Understanding diffusion models towards adversarial robustness. *arXiv preprint arXiv:2211.00322*, 2022.

Jongmin Yoon, Sung Ju Hwang, and Juho Lee. Adversarial purification with score-based generative models. In *International Conference on Machine Learning*, pp. 12062–12072. PMLR, 2021.

Sergey Zagoruyko and Nikos Komodakis. Wide residual networks. *arXiv preprint arXiv:1605.07146*, 2016.

Hongyang Zhang, Yaodong Yu, Jiantao Jiao, Eric Xing, Laurent El Ghaoui, and Michael Jordan. Theoretically principled trade-off between robustness and accuracy. In *International conference on machine learning*, pp. 7472–7482. PMLR, 2019.

Mingkun Zhang, Jianing Li, Wei Chen, Jiafeng Guo, and Xueqi Cheng. Classifier guidance enhances diffusion-based adversarial purification by preserving predictive information, 2024. URL https://openreview.net/forum?id=qvLPtx52ZR.

A INFLUENCE OF EOT ITERATIONS ON DBP ROBUSTNESS EVALUATION

In this section, we examine how the number of EoT iterations influences the DBP robustness evaluation. As previously discussed in Section 4.1, the Deterministic White-box attack could find the most effective attack direction. To quantify the impact of EoT iterations, we compare the attack direction of the standard White-box-EoT across various numbers of EoT iterations with that of the Deterministic White-box.

See Figure 7 for a visual explanation, where the red line shows the classification accuracy, and the blue line shows the similarity between the attack directions of the White-box-EoT and Deterministic White-box. The results show a clear trend: increasing the EoT iterations raises the similarity between the attack directions and reduces model accuracy.

Note that both the increase in similarity and the decline in accuracy converge as the number of iterations increases. Balancing computational cost and evaluation accuracy, we adopted the PGD20-EoT10 configuration for our robustness evaluation.

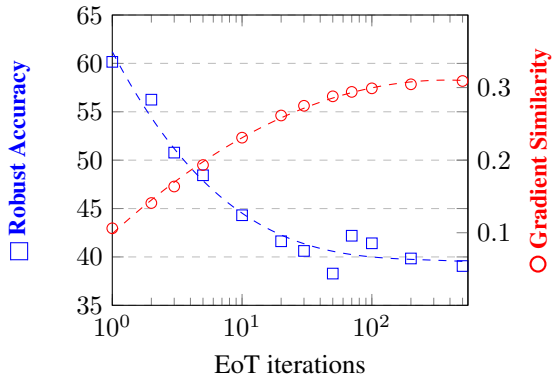

Figure 7: Robust accuracy (%) and gradient similarity on DP_{DDPM} for CIFAR-10, obtained by different EoT iterations. As the number of EoT iterations increases, the gradient similarity between the White-box-EoT attack direction and the Deterministic White-box attack direction increases and the robust accuracy decreases.

B DBP MODELS WITH DIFFERENT STOCHASTIC ELEMENTS CANNOT BE ATTACKED SIMULTANEOUSLY

Previous research has raised concerns about whether stochasticity enhances robustness, suggesting it may create obfuscated gradients that provide a false sense of security (Athalye et al., 2018a). To investigate this, we implement DW_{Semi}-box, a semi-stochastic framework that restricts the available stochastic elements to a limited set of options, in order to explore whether stochasticity can genuinely improve robustness.

$\text{DW}_{\text{semi-128}}$ builds on the concept of Deterministic White-box. In contrast to the Deterministic White-box approach, where the attacker exploits the exact stochastic noise used during evaluation, $\text{DW}_{\text{semi-128}}$ limits the stochastic elements to a constrained set of possibilities. To mount an attack across 128 distinct sets of stochastic noise, the attacker can employ the average adversarial direction across these 128 noise settings (EoT-128) to perturb the DBP model. We evaluate the impact of stochasticity by comparing the loss changes under DW-box and $\text{DW}_{\text{semi-128}}$ attacks. This is done by adjusting a factor k to modify an image $\boldsymbol{x}$ with a perturbation $\boldsymbol{\sigma}$, and evaluating the loss at $\boldsymbol{x} + k\boldsymbol{\sigma}$ for k ranging from -16 to 16. Perturbations are generated using the l_∞ Fast Gradient Sign Method (FGSM) (Goodfellow et al., 2015) with a magnitude of $1/255$. The experiment is conducted using the WideResNet-28-10 with DP_{DDPM} over the first 128 images from the CIFAR-10 dataset.

As shown in Figure 8, in the Deterministic White-box setting, perturbations lead to a significant increase in loss, demonstrating their effectiveness. However, under $\text{DW}_{\text{semi-128}}$, the loss increase is more moderate. This suggests that even when stochastic elements are limited to a small set of

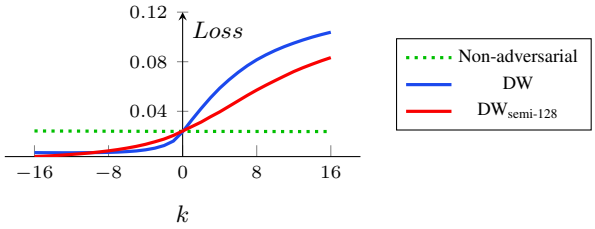

Figure 8: Impact of stochasticity on perturbation efficacy. Perturbations created under the DW_{semi}-box setting are less effective compared to those under the DW-box setting. For non-adversarial perturbations, each element is randomly assigned a value of either $1/255$ or $-1/255$.

possibilities, and the attacker has fully considered all options, stochasticity still contributes to the robustness of the DBP model. These results contradict the hypothesis that there might be a universally vulnerable direction when DBP applies different stochastic elements, thereby challenging concerns about potential insecurity.

C Impact of Attackers' Knowledge on Robustness: Comparison of Attack Settings

This section explores how the robustness of diffusion-based models is affected by the levels of knowledge that attackers possess concerning stochastic components in diffusion processes. We analyze how the knowledge of forward and reverse diffusion processes impact model robustness in various attack settings.

C.1 Stochastic Elements in the Diffusion Processes

Unlike deterministic models, where outputs are solely determined by the inputs, diffusion models introduce stochastic elements that also influence the outcomes. To explain the attacker's knowledge, we first explain the stochastic components involved in diffusion processes.

In the **forward diffusion process**, Gaussian noise is incorporated into the input data to derive a noisy version $\boldsymbol{x}_t$:

$$\boldsymbol{x}_t = \sqrt{\bar{\alpha}_t}\,\boldsymbol{x} + \sqrt{1-\bar{\alpha}_t}\,\boldsymbol{\epsilon}_f, \tag{10}$$

where $\boldsymbol{\epsilon}_f \sim \mathcal{N}(\mathbf{0}, \boldsymbol{I})$ is sampled once per input.

In the **reverse diffusion process**, the model progressively denoises x_t through iterative steps. For the Denoising Diffusion Probabilistic Model (DDPM), the reverse process is inherently stochastic:

$$\boldsymbol{x}_{t-1} = \frac{1}{\sqrt{\alpha_t}}\left(\boldsymbol{x}_t - \frac{1-\alpha_t}{\sqrt{1-\bar{\alpha}t}}\boldsymbol{\epsilon}_{\boldsymbol{\theta}}(\boldsymbol{x}_t, t)\right) + \sigma_t \boldsymbol{\epsilon}_t, \tag{11}$$

where $\boldsymbol{\epsilon}_t \sim \mathcal{N}(0, I)$ is sampled at each reverse step. In contrast, for the Denoising Diffusion Implicit Model (DDIM), the reverse process is deterministic, and no noise $\{\boldsymbol{\epsilon}_t\}_{t=1}^T$ is added.

C.2 Attack Settings and Attacker Knowledge

We define four attack settings based on the information accessible to the attacker, particularly regarding the Gaussian noise variables involved in the diffusion process. Table 10 provides a summary of the attacker's knowledge in each setting.

In the conventional white-box attack setting, the attacker possesses comprehensive knowledge of the model architecture and parameters but lacks insight into the stochastic elements used during inference ($\boldsymbol{\epsilon}_f$ and $\{\boldsymbol{\epsilon}_t\}_{t=1}^T$). The DW_{Fwd} setting grants the attacker knowledge of the Gaussian noise in the forward diffusion process ($\boldsymbol{\epsilon}_f$). Conversely, the DW_{Rev} setting provides the attacker with knowledge of the Gaussian noise introduced during the reverse diffusion steps ($\{\boldsymbol{\epsilon}_t\}_{t=1}^T$). The DW_{Both} setting offers the attacker complete access to all stochastic elements, $\boldsymbol{\epsilon}_f$ and $\{\boldsymbol{\epsilon}_t\}_{t=1}^T$. By manipulating the

Table 10: Information accessible to the attacker in different attack settings. $\boldsymbol{\epsilon}_f$ denotes the Gaussian noise in the forward process, and $\{\boldsymbol{\epsilon}_t\}_{t=1}^T$ represents the Gaussian noise in the reverse process.

Attacker's Knowledge	White-box	DW_{Fwd}	DW_{Rev}	DW_{Both}
Model Architecture and Parameters	✓	✓	✓	✓
Input Images and Class Labels	✓	✓	✓	✓
Forward Process Noise $\boldsymbol{\epsilon}_f$	×	✓	×	✓
Reverse Process Noise $\{\boldsymbol{\epsilon}_t\}_{t=1}^T$	×	×	✓	✓

attacker's knowledge in this manner, we isolate the individual effects of the forward and reverse diffusion processes on model robustness.

C.3 Implications of the Attacker's Knowledge of Stochastic Elements

The attacker's capability to craft potent adversarial examples is significantly influenced by their knowledge of the stochastic elements in diffusion processes. When these elements are unknown to the attacker, they must independently sample noise variables, leading to discrepancies between their approximations and the actual behavior of the victim model. Conversely, if the attacker has access to the exact noise variables used during inference, they can accurately replicate the model's behavior, significantly enhancing the effectiveness of their attack.

Attacker Without Knowledge of Stochastic Elements. In scenarios where the attacker lacks access to the specific noise variables $\boldsymbol{\epsilon}_f$ and $\{\boldsymbol{\epsilon}_t\}_{t=1}^T$, the model's output becomes unpredictable from the attacker's perspective. Consequently, the attacker must optimize the expected value of the loss function over the distribution of these stochastic elements. The optimization problem for generating an adversarial example $\boldsymbol{x}^{\text{adv}}$ is formulated as:

$$\boldsymbol{x}^{\text{adv}} = \arg\max_{\|\boldsymbol{x}^{\text{adv}}-\boldsymbol{x}\|\leq\delta} \mathbb{E}_{\boldsymbol{\epsilon}_f,\{\boldsymbol{\epsilon}_t\}_{t=1}^T} \left[L\left(f(\boldsymbol{x}^{\text{adv}};\boldsymbol{\epsilon}_f,\{\boldsymbol{\epsilon}_t\}_{t=1}^T),y\right)\right], \tag{12}$$

where δ specifies the permissible perturbation magnitude, L is the loss function, f represents the model's output given the input and stochastic elements, and y is the actual class label.

Attacker With Knowledge of Stochastic Elements. If the attacker possesses precise knowledge of the noise variables $\boldsymbol{\epsilon}_f$ and $\{\boldsymbol{\epsilon}_t\}_{t=1}^T$ used during the model's inference, they can accurately replicate the behavior of the victim classifier. In this case, the stochastic processes become deterministic from the attacker's perspective, enabling the optimization problem to be formulated as:

$$\boldsymbol{x}^{\text{adv}} = \arg\max_{\|\boldsymbol{x}^{\text{adv}}-\boldsymbol{x}\|\leq\delta} L\left(f(\boldsymbol{x}^{\text{adv}};\boldsymbol{\epsilon}_f,\{\boldsymbol{\epsilon}_t\}_{t=1}^T),y\right). \tag{13}$$

This precise knowledge allows the attacker to adopt the exact noise that will be used during the target evaluation, allowing effective evaluation.

C.4 Effect of Attacker's Knowledge on Model Robustness

We test the robustness of DDPM under these four settings, and Table 11 encapsulates the result.

Table 11: Robust accuracy (%) of DDPM under different attack settings.

Attack Setting	Robust Accuracy (l_∞)
Conventional White-Box Attack	47.27
DW_{Fwd}	45.41
DW_{Rev}	35.25
DW_{Both}	16.80

Conventional White-Box Attack. In this setting, the attacker has full knowledge of the model's architecture and parameters but lacks access to the stochastic components ($\boldsymbol{\epsilon}_f$ and $\{\boldsymbol{\epsilon}_t\}_{t=1}^T$) involved during inference. Hence, the model's output is unpredictable due to the stochasticity of both diffusion processes, making it challenging for the attacker to generate effective adversarial examples (reaching robust accuracy of **47.27%**).

DW$_{\text{Fwd}}$. Here, the attacker is aware of the Gaussian noise $\boldsymbol{\epsilon}_f$ used in the forward diffusion process but does not have knowledge of the noise $\{\boldsymbol{\epsilon}_t\}_{t=1}^T$ used in the reverse process. This partial information enables the attacker to replicate the forward process, reducing uncertainty. However, the reverse process remains unpredictable. The exposure of the forward process leads to a slight decrease in robust accuracy to **45.41%**.

DW$_{\text{Rev}}$. In this case, the attacker knows the noise variables $\{\boldsymbol{\epsilon}_t\}_{t=1}^T$ used in the reverse diffusion process but lacks knowledge of the forward process noise $\boldsymbol{\epsilon}_f$. This enables the attacker to align their strategy more closely with the behavior of the model during the reverse diffusion phase, resulting in a more substantial drop in robust accuracy to **35.25%**. These findings suggest that the stochasticity of the reverse process plays a more critical role in maintaining model robustness than that of the forward process.

DW$_{\text{Both}}$. In this case, the attacker possesses full knowledge of the noise variables for both the forward and reverse diffusion processes, allowing them to precisely replicate both processes and eliminate stochasticity from their perspective. This complete predictability enables the attacker to craft highly effective adversarial examples, leading to a significant reduction in robust accuracy to **16.80%**. These results underscore the importance of the stochastic elements in preserving model robustness; when fully exposed, the model's defense mechanisms are substantially weakened.

D The Role of Stochasticity in DBP Compared to Certified Defense Methods

In this appendix section, we delve deeper into the role of randomness in Diffusion-Based Prediction (DBP) models and contrast it with its role in certified defense methods such as randomized smoothing (Cohen et al., 2019). While both approaches incorporate stochasticity, their mechanisms and implications for adversarial robustness differ significantly.

- Conventionally, the classification models discussed in the studies of adversarial robustness can be viewed as mappings from input space $\mathcal{X}$ to the label space $\mathcal{Y}$. However, DBP additionally involves a random variable $\boldsymbol{\epsilon} \in \mathcal{E}$ that determines the random sampling in the forward and reverse processes (which can be the random seed in implementation). Hence, a DBP model protected classifier f can be viewed as the mapping $f : (\mathcal{X}, \mathcal{E}) \to \mathcal{Y}$.
- Previous studies on randomized smoothing treat the randomized model f as a mapping $f : \mathcal{X} \to \mathcal{P}_{\mathcal{Y}}$, where $\mathcal{P}_{\mathcal{Y}}$ is the space of label distribution. Typically, the final prediction can be formulated as $F(\boldsymbol{x}) = \arg\max_c [f(\boldsymbol{x})]_c$, i.e., the class c with the highest probability in the output distribution $\mho(\boldsymbol{x})$. Apparently, F deterministically maps $\mathcal{X}$ to $\mathcal{Y}$, consistent with the conventional models.
- Recent studies on DBP also regard the model as $f : \mathcal{X} \to \mathcal{P}_{\mathcal{Y}}$, without explicitly studying the role of $\boldsymbol{\epsilon}$. *The key difference between DBP and randomized smoothing is that the final prediction for an input $\boldsymbol{x}$ is directly sampled from the distribution $f(\boldsymbol{x})$ for once, instead of sampling multiple times to approximate $F(\boldsymbol{x})$ as in randomized smoothing*.
- In this paper, we revisit DBP by treating the randomized model f as the mapping $f : \mathcal{X}, \mathcal{E}) \to \mathcal{Y}$ and studying the role of $\boldsymbol{\epsilon} \in \mathcal{E}$ as an input of f. From this perspective, the conventional adversarial setting assuming full knowledge of the model parameters (but not $\boldsymbol{\epsilon}$) is not a complete white box, which motivates us to study the DW-box setting.
- From our perspective, we can clearly point out the difference between DBP and randomized smoothing in terms of the loss landscape. Given an input $\boldsymbol{x}_0$, the local loss landscape for a DBP model f is not deterministic as it also depends on $\boldsymbol{\epsilon}$. *Although the expected loss landscape over $\boldsymbol{\epsilon} \in \mathcal{E}$ may be smooth, it does not suggest the robustness of DBP, as $\boldsymbol{\epsilon}$ is fixed during a single inference run of DBP*. Indeed, our study suggests that given $\boldsymbol{x}_0$ and a fixed $\boldsymbol{\epsilon}_0$, the local landscape of DBP is likely not smooth. In contrast, the loss landscape of a randomized smoothing model F may be smooth as it is the average landscape over multiple $\boldsymbol{\epsilon}$. To conclude, we argue that the random noise itself may not smooth the loss landscape, but the average over random noises may.

E EVALUATION SETTINGS

Previous assessments of DBP robustness have often utilized potentially unreliable methods. In particular, due to the iterative denoising process in diffusion models, some studies resort to mathematical approximations of gradients to reduce memory constraints (Nie et al., 2022) or to circumvent the diffusion process during backpropagation (Wang et al., 2022). Furthermore, the reliability of AutoAttack, a widely used evaluation method, in assessing the robustness of DBP models is questionable. Although AutoAttack includes a *Rand* version designed for stochastic models, Nie et al. (2022) have found instances where the *Rand* version is less effective than the *Standard* version in evaluating DBP robustness.

To improve the robustness evaluation of diffusion-based purification (DBP) models, we implement several modifications. First, to ensure the accuracy of the gradient computations, we compute the exact gradient of the entire diffusion classification pipeline. To mitigate the high memory requirements in diffusion iterative denoising steps, we use gradient checkpointing (Chen et al., 2016) techniques to optimize memory usage. In addition, to deal with the stochastic nature of the DBP process, we incorporate the Expectation over Transformation (EoT) method to average gradients across different attacks. We adopt EoT with 10 iterations, and a detailed discussion of the choice of EoT iterations can be found in Appendix A. We also use the Projected Gradient Descent (PGD) attack instead of AutoAttack for our evaluations. We discover a bug in the *Rand* version of AutoAttack that causes it to overestimate the robustness of DBP. After fixing this, $\text{AutoAttack}_{\text{Fixed}}$ gives similar results to PGD attacks, but at a much higher computational cost. Our revised robustness evaluation revealed that DBP models, such as DiffPure and GDMP, perform worse than originally claimed. DiffPure's accuracy dropped from a claimed 70.64% to an actual 55.96%, and GDMP's from 90.10% to 40.97%. These results emphasize the urgent need for more accurate and reliable evaluation methods to properly assess the robustness of DBP models. Similar evaluation protocols are also applied in Chen et al. (2023); Kang et al. (2024).

E.1 EVALUATION WITH FIXED AUTOATTACK

AutoAttack (Croce & Hein, 2020), an ensemble of White-box and Black-box attacks, is a popular benchmark for evaluating model robustness. It is used in RobustBench (Croce et al., 2020) to evaluate over 120 models. However, Nie et al. (2022) finds that the *Rand* version of AutoAttack, designed to evaluate stochastic defenses, sometimes yields higher accuracy than the *Standard* version that is intended for deterministic methods. Our comparison of AutoAttack and PGD20-EoT10 in Table 12 also shows that the *Rand* version of AutoAttack gives higher accuracy than the PGD20-EoT10 attack.

We attribute this to the sample selection of AutoAttack. As an ensemble of attack methods, AutoAttack selects the final adversarial sample from either the original input or the attack results. However, the original implementation neglects stochasticity and considers a adversarial sample to be sufficiently adversarial if it gives a false result in one evaluation. To fix this, we propose a 20-iteration evaluation and selects the adversarial example with the lowest accuracy. The flawed code is in the official GitHub main branch, git version $a39220048b3c9f2cca9a4d3a54604793c68eca7e$, and specifically in lines #125, #129, #133-136, #157, #221-225, #227-228, #231 of the file 'autoattack/autoattack.py'. We will open source our updated code and encourage future stochastic defense methods to be evaluated against the fixed code. The code now can be found at: https://github.com/Buntender/auto-attack.

Following the fix, robust accuracy under $\text{AutoAttack}_{\text{Fixed}}$ decreases by up to 10 points, producing results comparable to our PGD20-EoT10 test outcomes. However, using AutoAttack on DP_{DDPM} took nearly 25 hours, five times longer than PGD20-EoT10. Therefore, we will use PGD20-EoT10 for most robustness evaluation.

F EXPERIMENTAL SETTING OF VISUALIZATION OF THE ATTACK TRAJECTORY

We visualize the attack by plotting the loss landscape and trace the trajectories of EoT attack under White-box setting and the Deterministic White-box setting in Figure 3. We run a vanilla PGD20-EoT10 attack under White-box setting and a PGD20 attack under Deterministic White-box setting. We then expand a 2D space using the final perturbations from these two attacks, draw the loss landscape, and plot the attack trajectories on it. Note that the two adversarial perturbation directions

Table 12: AutoAttack (*Rand* version) and PGD20-EoT10 performance on DBP methods for CIFAR-10 (the lower the better). The original AutoAttack produces high accuracy (%), after fixing, it achieves similar results to PGD20+EoT10 attack.

DBP method	l_∞			l_2		
	AutoAttack	$\text{AutoAttack}_{\text{Fixed}}$	PGD20-EoT10	AutoAttack	$\text{AutoAttack}_{\text{Fixed}}$	PGD20-EoT10
DiffPure	62.11	56.25	**55.96**	81.84	76.37	**75.78**
DP_{DDPM}	57.81	**46.88**	48.63	71.68	**71.09**	72.27
DP_{DDIM}	50.20	**40.62**	44.73	77.15	**70.70**	71.68

Table 13: Clean and robust accuracy (%) on different DBP methods for CIFAR-10, evaluated with $\text{AutoAttack}_{\text{Fixed}}$ (*Rand* version). All methods show consistent improvement when fine-tuned with ADDT.

DBP method	Vanilla			ADDT		
	Clean	ℓ_∞	ℓ_2	Clean	ℓ_∞	ℓ_2
DiffPure	89.26	56.25	76.37	89.94	**58.20**	**77.34**
DP_{DDPM}	85.94	46.88	71.09	85.64	**48.63**	**72.27**
DP_{DDIM}	88.38	40.62	70.70	88.77	**44.73**	**71.68**

are not strictly orthogonal. To extend this 2D space, we use the Deterministic White-box attack direction and the orthogonal component of the EoT attack direction. Note that the endpoints of both trajectories lie exactly on the loss landscape, while intermediate points are projected onto it. The plot is evaluated using WideResNet-28-10 with DP_{DDPM} over the first 128 images of CIFAR-10 dataset.

G PSEUDO-CODE OF ADDT

The pseudo-code for adopting ADDT within DDPM and DDIM framework is shown in Algorithm 1.

Algorithm 1 Adversarial Denoising Diffusion Training (ADDT)

Require: $\boldsymbol{x}_0$ is image from training dataset, y is the class label of the image, C is the classifier, $\boldsymbol{P}$ is one-step diffusion reverse process and $\boldsymbol{\theta}$ is it's parameter, L is CrossEntropy Loss.

1: **for** $\boldsymbol{x}_0$, y in the training dataset **do**
2: $t \sim \mathcal{U}(\{1, \ldots, T\})$
3: $\lambda_t = \texttt{clip}(\gamma_t \lambda_{\text{unit}}, \lambda_{\text{min}}, \lambda_{\text{max}})$, where $\gamma_t = \frac{\sqrt{\overline{\alpha}_t}}{\sqrt{1-\overline{\alpha}_t}}$
4: Init $\boldsymbol{\delta}$ to a small random vector.
5: **for** 1 to $\text{ADDT}_{\text{iterations}}$ **do**
6: $\boldsymbol{\epsilon} \sim \mathcal{N}(0, I)$
7: $\boldsymbol{\epsilon}' = \texttt{RBGM}(\boldsymbol{\delta}, \boldsymbol{\epsilon})$
8: $\boldsymbol{x}_t = \sqrt{\overline{\alpha}_t}\boldsymbol{x}_0 + \sqrt{1-\lambda_t^2}\sqrt{1-\overline{\alpha}_t}\boldsymbol{\epsilon} + \lambda_t\sqrt{1-\overline{\alpha}_t}\boldsymbol{\epsilon}'$
9: $\boldsymbol{\delta} = \boldsymbol{\delta} + \nabla_{\boldsymbol{\epsilon}'} L(C(\boldsymbol{P}(\boldsymbol{\theta}, \boldsymbol{x}_t, t), y))$
10: **end for**
11: $\boldsymbol{\epsilon} \sim \mathcal{N}(0, I)$
12: $\boldsymbol{\epsilon}' = \texttt{RBGM}(\boldsymbol{\delta}, \boldsymbol{\epsilon})$
13: $\boldsymbol{x}_t = \sqrt{\overline{\alpha}_t}\boldsymbol{x}_0 + \sqrt{1-\lambda_t^2}\sqrt{1-\overline{\alpha}_t}\boldsymbol{\epsilon} + \lambda_t\sqrt{1-\overline{\alpha}_t}\boldsymbol{\epsilon}'$
14: Take a gradient descent step on:
$\nabla_{\boldsymbol{\theta}} \| \frac{\sqrt{\overline{\alpha}_t}}{\sqrt{1-\overline{\alpha}_t}}(\boldsymbol{x}_0 - \boldsymbol{P}(\boldsymbol{\theta}, \boldsymbol{x}_t, t)) \|_2^2$
15: **end for**

Diffusion model $\boldsymbol{\epsilon}_{\boldsymbol{\theta}}$ predicts the Gaussian noise added to the image, adopting Equation (4) in the paper, we have $\boldsymbol{P}(\boldsymbol{\theta}, \boldsymbol{x}_t, t) = \left(\boldsymbol{x}_t - \sqrt{1-\overline{\alpha}_t}\boldsymbol{\epsilon}_{\boldsymbol{\theta}}(\boldsymbol{x}_t, t)\right) / \sqrt{\overline{\alpha}_t}$

H ADDT RESULTS ON DP_{DDIM}

As shown in Table 14, the performance of DP_{DDIM} is less sensitive to the number of function evaluations (NFEs). Additionally, ADDT consistently improved the robustness of DP_{DDIM}.

Table 14: Clean and robust accuracy (%) on DP_{DDIM}. ADDT improve robustness across different NFEs (*: default DDIM generation setting, -: classifier only).

Dataset	NFEs	Vanilla			ADDT		
		Clean	l_∞	l_2	Clean	l_∞	l_2
CIFAR-10	-	95.12	0.00	1.46	95.12	0.00	1.46
	5	89.65	42.19	68.65	88.57	**47.27**	**70.61**
	10*	88.96	43.16	67.58	88.18	**47.85**	**70.61**
	20	87.89	41.70	69.24	88.67	**48.63**	**69.73**
	50	88.96	42.48	68.85	88.57	**46.68**	**69.24**
	100	88.38	42.19	70.02	88.77	**46.48**	**71.19**
CIFAR-100	-	76.66	0.00	2.44	76.66	0.00	2.44
	5	62.11	15.43	35.74	62.79	**17.58**	**38.87**
	10*	62.21	15.33	36.52	64.45	**20.02**	**39.26**
	20	63.67	15.62	37.89	65.23	**18.65**	**40.62**
	50	62.40	16.31	37.79	63.87	**19.14**	**39.94**
	100	63.28	15.23	36.62	66.02	**18.85**	**39.84**

I ADOPTING VPSDE(DDPM++) AND EDM MODELS IN DBP

In the previous discussion of the robustness of DBP models, as detailed in Section 4.1, our focus was primarily on the DDPM and DDIM models. We now extend our analysis to include VPSDE (DDPM++) and EDM (Karras et al., 2022) models. VPSDE (DDPM++) is the diffusion model used in DiffPure.

From a unified perspective, diffusion process can be modeled by stochastic differential equations (SDE) (Song et al., 2021b). The forward SDE, as described in Equation (14), converts a complex initial data distribution into a simpler, predetermined prior distribution by progressively infusing noise. This can also be done in a single step, as shown in Equation (15), mirroring the strategy of DDPM described in Equation (2). Reverse SDE, as explained in Equation (16), reverses this process, restoring the noise distribution to the original data distribution, thus completing the diffusion cycle.

$$\mathrm{d}\boldsymbol{x} = \boldsymbol{f}(\boldsymbol{x}, t)\mathrm{d}t + g(t)\mathrm{d}\boldsymbol{w}, \tag{14}$$

$$\begin{aligned} &p_{0t}(\boldsymbol{x}(t) \mid \boldsymbol{x}(0)) = \\ &\quad \mathcal{N}\left(\boldsymbol{x}(t); e^{-\frac{1}{4}t^2(\bar{\beta}_{\max}-\bar{\beta}_{\min})-\frac{1}{2}t\bar{\beta}_{\min}}\boldsymbol{x}(0), \boldsymbol{I} - \boldsymbol{I}e^{-\frac{1}{2}t^2(\bar{\beta}_{\max}-\bar{\beta}_{\min})-t\bar{\beta}_{\min}}\right), \quad t \in [0,1] \end{aligned} \tag{15}$$

$$\mathrm{d}\boldsymbol{x} = \left[\boldsymbol{f}(\boldsymbol{x}, t) - g^2(t)\nabla_{\boldsymbol{x}} \log p_t(\boldsymbol{x})\right]\mathrm{d}t + g(t)\mathrm{d}\bar{\boldsymbol{w}}. \tag{16}$$

The reverse process of SDEs also derives equivalent ODEs Equation (17) for fast sampling and exact likelihood computation, and this Score ODEs corresponds to DDIM.

$$\mathrm{d}\boldsymbol{x} = \left[\boldsymbol{f}(\boldsymbol{x}, t) - \frac{1}{2}g(t)^2\nabla_{\boldsymbol{x}} \log p_t(\boldsymbol{x})\right]\mathrm{d}t. \tag{17}$$

By modulating the stochasticity, we can craft a spectrum of semi-stochastic models that bridge pure SDEs and deterministic ODEs, offering a range of stochastic behaviors.

EDM provides a unified framework to synthesize the design principles of different diffusion models (DDPM,DDIM,iDDPM (Nichol & Dhariwal, 2021),VPSDE,VESDE (Song et al., 2021b)). Within this framework, EDM incorporates efficient sampling methods, such as the Heun sampler, and introduces optimized scheduling functions $\sigma(t)$ and $s(t)$. This allows EDM to achieve state-of-the-art performance in generative tasks.

EDM forward process could be presented as:

$$\boldsymbol{x}_t = \boldsymbol{x}_0 + \sigma(t^*)\boldsymbol{\epsilon}, \quad \boldsymbol{\epsilon} \sim \mathcal{N}(\mathbf{0}, \boldsymbol{I}), \tag{18}$$

where we choose $\sigma(t^*) = 0.5$ for clean and robust accuracy tradeoff. And for reverse process, EDM incorporates a parameter S_{churn} to modulate the stochastic noise infused during the reverse process. For our experiments, we choose 50 reverse steps (50 NFEs, NFEs is Function of Neural Function Evaluations), configured the parameters with $S_{min} = 0.01$, $S_{max} = 0.46$, $S_{noise} = 1.007$, and designate $S_{churn} = 0$ to represent EDM-ODE, $S_{churn} = 6$ to represent EDM-SDE.

As shown in Table 15, our ADDT could also increase the robustness of DP_{EDM}.

Table 15: Clean and robust accuracy (%) on DP_{EDM} for CIFAR-10. ADDT improves robustness in both $\text{DP}_{\text{EDM-SDE}}$ and $\text{DP}_{\text{EDM-ODE}}$.

Metric	Vanilla		ADDT	
	$\text{DP}_{\text{EDM-SDE}}$	$\text{DP}_{\text{EDM-ODE}}$	$\text{DP}_{\text{EDM-SDE}}$	$\text{DP}_{\text{EDM-ODE}}$
Clean	86.43	87.99	86.33	87.99
ℓ_∞	62.50	60.45	**66.41**	**64.16**
l_2	76.86	75.49	**79.16**	**77.15**

J Strengthening DBP via Augmented Stochasticity

(Song et al., 2021b) present a Predictor-Corrector sampler for SDEs reverse process for VPSDE (DDPM++), as detailed in Appendix I. However, standard implementations of VPSDE (DDPM++) typically use only the Predictor. Given our hypothesis that stochasticity contributes to robustness, we expect that integrating the Corrector sampler into VPSDE (DDPM++) would further enhance the robustness of DBP models. Our empirical results, as shown in Table 16, confirm that the inclusion of a Corrector to VPSDE (DDPM++) indeed improve the model's defenses ability against adversarial attacks with ℓ_∞ norm constraints. This finding supports our claim that the increased stochasticity can further strengthen DBP robustness. Adding Corrector is also consistent with ADDT. Note that the robustness against ℓ_2 norm attacks does not show a significant improvement with the integration of the Extra Corrector. A plausible explanation for this could be that the robustness under ℓ_2 attacks is already quite strong, and the compromised performance on clean data counteracts the increase in robustness.

Table 16: Clean and robust accuracy (%) on $\text{DP}_{\text{DDPM++}}$ for CIFAR-10. Both extra Corrector and ADDT fine-tuning improved robustness.

Metric	Vanilla	Extra Corrector	ADDT	ADDT+Extra Corrector
Clean	89.26	85.25	89.94	85.55
ℓ_∞	55.96	59.77	62.11	**65.23**
ℓ_2	75.78	74.22	**76.66**	**76.66**

K Discussion about RBGM-Mapped Perturbations

K.1 Motivation and Advantages of RBGM

To elaborate, a conventional diffusion forward process is based on the equation:

$$\boldsymbol{x}_t = \sqrt{\overline{\alpha}_t}\,\boldsymbol{x}_0 + \sqrt{1 - \overline{\alpha}_t}\,\boldsymbol{\epsilon}, \tag{19}$$

where $\boldsymbol{x}_t$ represents the noisy image at time t, $\boldsymbol{x}_0$ is the initial input, $\overline{\alpha}_t$ is a time-dependent scaling factor, and $\boldsymbol{\epsilon}$ is random Gaussian noise. Our proposed method, ADDT, modifies this equation to include an adversarial component:

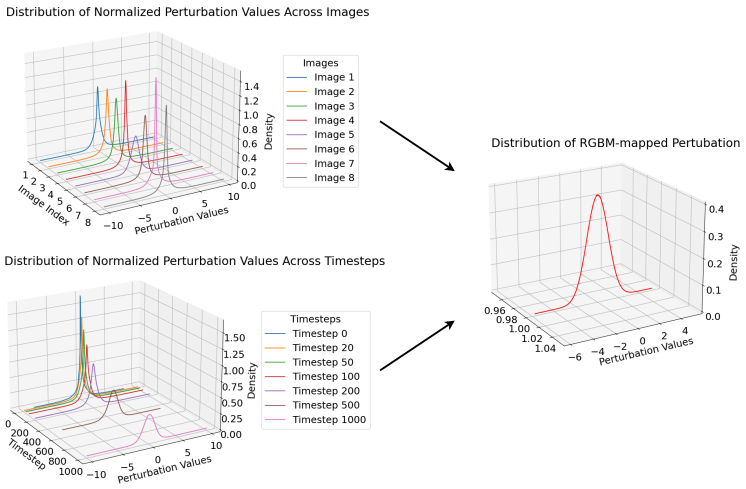

Figure 9: Raw perturbation values exhibit diverse distributions across images and time steps. RBGM maps these perturbations to a uniform Gaussian distribution.

$$\boldsymbol{x}_t = \sqrt{\overline{\alpha}_t}\,\boldsymbol{x}_0 + \sqrt{1-\lambda_t^2}\,\sqrt{1-\overline{\alpha}_t}\,\boldsymbol{\epsilon} + \lambda_t\,\sqrt{1-\overline{\alpha}_t}\,\boldsymbol{\epsilon}_{\boldsymbol{\delta}}(\boldsymbol{\delta}). \tag{20}$$

In this revised formulation, $\boldsymbol{\epsilon}_{\boldsymbol{\delta}}(\boldsymbol{\delta})$ represents the adversarial perturbation, and λ_t is a parameter that controls the blend between traditional and adversarial noise. The core objective of ADDT training is to *generate perturbations that emulate the characteristics of Gaussian noise in conventional diffusion training while incorporating adversarial disturbances*. This leads to our Rank-Based Gaussian Mapping (RBGM) technique, which preserves the relative ordering of perturbation magnitudes while adjusting their values to more closely resemble a Gaussian distribution. The advantages of RBGM are twofold:

Enhancing statistical consistency. Raw adversarial perturbation values often exhibit non-standard distributions, and RBGM serves to recalibrate these perturbations, aligning them more closely with a Gaussian distribution. To elaborate, rather than enforcing a multivariate Gaussian distribution for the entire perturbation, RBGM ensures that the distribution of individual perturbation values adheres to Gaussian characteristics.

The benefit of this transformation can be illustrated in Figure 9 and Figure 10. For a fair comparison, the perturbation values have been normalized. In Figure 9, the original perturbation values display a wide array of distributions across different images and time steps. After the mapping of RBGM, these values are transformed to exhibit a uniform Gaussian distribution.

In Figure 10, the raw perturbations show irregular and inconsistent behavior when mixed with Gaussian noise at varying ratios. However, after RBGM mapping, the perturbations and the mixture exhibit consistent statistics with the pure Gaussian noise. The statistical consistency of the perturbation values may ease the training of the diffusion model and avoid significant deviation from the normal diffusion process.

Reducing image-specific dependence. In the training of diffusion models, the Gaussian noise is independent of specific images or time steps. This characteristic contrasts with adversarial perturbations, which are typically tailored to each input. RBGM addresses this issue by introducing stochasticity into the construction of perturbations while preserving the ranks of the values of the image-dependent adversarial perturbations. This approach effectively reduces image-specific dependence. Consequently, RBGM enhances ADDT's ability to better mimic the diffusion training process and potentially mitigates the overfitting of training images.

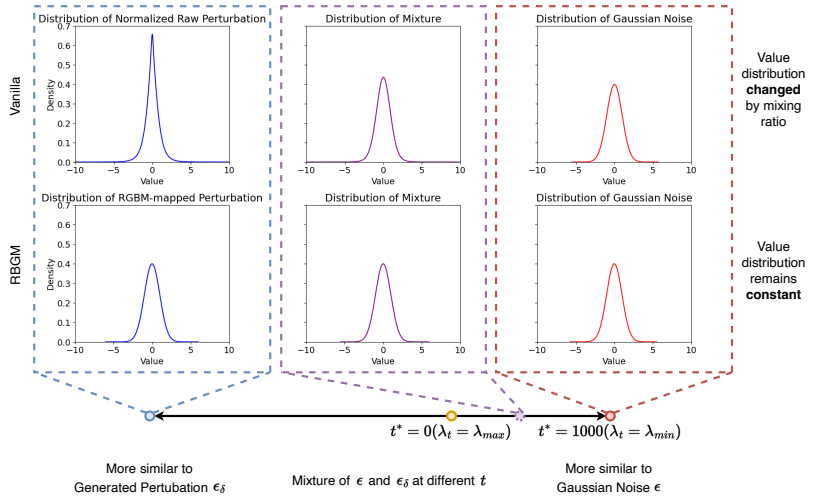

Figure 10: RBGM ensures that mixing perturbations with Gaussian noise at any ratio yields a consistent value distribution.

K.2 RBGM-Mapped Perturbations Preserve Adversarial Characteristics

While RBGM-mapped perturbations are "selected from a Gaussian distribution", their actual distribution deviates from a pure Gaussian distribution, and are adversarial for models. To substantiate this claim, we compare the influence of RBGM-mapped perturbations and Gaussian noise on model performance. In our experiments, we perturb clean images by adding RBGM-mapped perturbations and Gaussian noise, each scaled by a factor of 0.03. The results present in Table 17 demonstrate that RBGM-mapped perturbations effectively act as adversarial inputs to the model. These perturbations drastically reduce the accuracy of a pre-trained clean WRN-28-10 from 95.12% to 4.47%.

Table 17: Comparison of model accuracy % under different conditions. RBGM-mapped perturbations lead to a significant reduction in accuracy compared to Gaussian noise.

Classifier	Clean	Gaussian noise	RBGM-mapped perturbation
WRN-28-10	95.12	81.54	4.47

K.3 Blending Adversarial Perturbations into Diffusion Model Training

In conventional adversarial attacks, perturbations are directly applied to the image, resulting in an adversarial image:

$$\boldsymbol{x}_{\text{adv}} = \boldsymbol{x}_0 + \boldsymbol{\delta},$$

where $\boldsymbol{x}_0$ is the original input image, and $\boldsymbol{\delta}$ is the adversarial perturbation. In ADDT, we incorporate this concept into the diffusion process, redefining the noisy image at time step t as:

$$\boldsymbol{x}_t = \sqrt{\overline{\alpha}_t}(\boldsymbol{x}_0 + \boldsymbol{\delta}) + \sqrt{1 - \overline{\alpha}_t}\boldsymbol{\epsilon}, \tag{21}$$

To enable the diffusion model to effectively purify adversarial perturbations during training, we reformulate the above equation by merging the perturbation $\boldsymbol{\delta}$ with the noise $\boldsymbol{\epsilon}$. This results in:

$$\boldsymbol{x}_t = \sqrt{\overline{\alpha}_t}\,\boldsymbol{x}_0 + \sqrt{1 - \overline{\alpha}_t}\,\left(\boldsymbol{\epsilon} + \gamma_t\,\boldsymbol{\delta}\right), \tag{22}$$

where γ_t is a scaling factor defined as:

$$\gamma_t = \frac{\sqrt{\overline{\alpha}_t}}{\sqrt{1 - \overline{\alpha}_t}}. \tag{23}$$

Since $\overline{\alpha}_t$ is a time-dependent parameter that monotonically decreases from 1 to 0 during the diffusion process, γ_t spans the range from 0 to ∞. To ensure the adversarial perturbation remains within a manageable intensity, we constrain its value to the range between λ_{min} and λ_{max}.

K.4 RBGM ENHANCES PERTURBATION COMPATIBILITY WITH DIFFUSION MODEL TRAINING

To illustrate how RBGM enhances the compatibility of perturbations with diffusion model training, we conduct comparative analyses in two scenarios. First, we assess the impact of RBGM on statistical consistency by comparing Gaussian noise with adversarial perturbations reordered based on Gaussian noise ranks. Second, we evaluate the effectiveness of RBGM-mapped perturbations in improving model robustness while maintaining generative performance by comparing them with ℓ_2-normalized perturbations.

Gaussian noise vs. adversarial perturbations ordered by Gaussian noise We begin by examining RBGM's influence on statistical consistency through two training methodologies:

1. **Vanilla**: Trained with standard Gaussian noise.
2. **ADDT$_{\text{Gaussian reordered}}$**: Trained with adversarial perturbations reordered according to Gaussian noise ranks. To ensure a fair comparison, the perturbations are normalized to have a mean of 0 and a variance of 1, as their original magnitudes (derived from accumulated gradients) are significantly smaller than those of standard Gaussian noise. Note that this approach—reordering adversarial perturbations based on Gaussian noise ranks—is distinct from RBGM, where Gaussian noise is reordered based on adversarial perturbation ranks.

The results presented in Table 18 reveal that models trained with Gaussian noise reordering using adversarial perturbation values exhibit lower accuracy on both clean and adversarial samples compared to vanilla models. This decline in performance underscores RBGM's ability to enhance perturbation compatibility with diffusion model training by improving statistical consistency.

Table 18: Comparison of DP$_{\text{DDPM}}$ accuracy under different conditions and perturbation types. Training with perturbations reordered by Gaussian noise and adversarial perturbation values degrades performance.

NFEs	Vanilla			ADDT$_{\text{Gaussian reordered}}$		
	Clean	ℓ_∞	ℓ_2	Clean	ℓ_∞	ℓ_2
5	49.51	**21.78**	**36.13**	48.40	21.10	33.40
10	73.34	**36.72**	**55.47**	71.78	34.07	52.98
20	81.45	**45.21**	**65.23**	79.99	42.43	64.21
50	85.54	**46.78**	**68.85**	83.90	46.73	68.17
100*	85.94	**47.27**	**69.34**	84.54	46.98	69.33

RBGM-mapped perturbations vs. ℓ_2-normalized perturbations To further investigate RBGM's effectiveness in making adversarial perturbations compatible with diffusion model training, we compare:

1. **ADDT**: Trained with RBGM-mapped perturbations.
2. **ADDT$_{\ell_2\text{-normalized}}$**: Trained with raw adversarial perturbations, scaled to match the ℓ_2 norm of standard Gaussian noise. This scaling ensures that the perturbations share the same ℓ_2 norm as those mapped by RBGM, which we refer to as ℓ_2-normalized perturbations.

As shown in Table 19, models trained with ℓ_2-normalized perturbations tend to perform better under ℓ_2 attacks in some scenarios (possibly because these perturbations are more similar to those generated by ℓ_2 attack during testing). ADDT generally achieves better results. This advantage is particularly pronounced under ℓ_∞ attacks and in scenarios with higher NFEs. Furthermore, as shown in Table 20, ADDT yields a lower FID value, reflecting better preservation of generative capabilities.

As discussed in Appendix K.1, the goal of utilizing RGBM to generate perturbations is to mimic the characteristic of Gaussian noise, hence aligning ADDT closer to traditional diffusion model training. In this context, both RBGM and ℓ_2 normalization serve as approximations of Gaussian noise. Yet, RBGM provides a more precise approximation, enhancing robustness and maintaining the generative performance more effectively than ℓ_2 normalization.

Table 19: Comparison of DP_{DDPM} accuracy under different perturbation conditions. Training with ADDT generally achieves better results. This advantage is particularly pronounced under ℓ_∞ attacks and in scenarios with higher NFEs.

NFEs	ADDT			$\text{ADDT}_{\ell_2\text{-normalized}}$		
	Clean	ℓ_∞	ℓ_2	Clean	ℓ_∞	ℓ_2
5	59.96	**30.27**	41.99	60.40	28.47	**44.58**
10	78.91	**43.07**	62.97	79.29	41.90	**63.72**
20	83.89	**48.44**	**69.82**	83.59	47.85	67.68
50	85.45	**50.20**	69.04	84.83	49.12	**69.24**
100*	85.64	**51.46**	**70.12**	84.97	49.95	69.29

Table 20: FID score of DDPM for CIFAR-10 fine-tuned under different conditions. Fine-tuning with ADDT result in lower FID score compared to ℓ_2 normalization.

	Clean fine-tuning	ADDT	$\text{ADDT}_{\ell_2\text{-normalized}}$
FID	3.50	5.190	5.678

L Comparing RBGM-Mapped Perturbations with l_∞ Perturbations

In Section 6.3, we briefly explore the generation capabilities of diffusion models trained with RBGM-mapped and l_∞ perturbations. Here, we provide further experiment and delve deeper into their robustness comparison. To train with l_∞ perturbations, we adjust ADDT, replacing RBGM-mapped perturbations with l_∞ perturbations. Here, instead of converting accumulated gradients to Gaussian-like perturbations, we use a 5-step projected gradient descent (PGD-5) approach. For fair comparison, we also set $\lambda_{unit} = 1, \lambda_{min} = 0, \lambda_{max} = 10$ and refer to this modified training protocol as $\text{ADDT}_{\ell_\infty}$.

We evaluate the clean and robust accuracy of ADDT and ADDT_{l_∞} fine-tuned models. These models exhibit different behaviors. As shown in Table 21, while Gaussian-mapped perturbations can simultaneously improve clean accuracy and robustness against both l_2 and l_∞ attacks, training with l_∞ perturbations primarily improves performance against l_∞ attacks.

Table 21: Clean and robust accuracy (%) on DBP models trained with different perturbations for CIFAR-10. While ADDT simultaneously improves clean accuracy and robustness against both l_2 and l_∞ attacks. ADDT_{l_∞} primarily improves performance against l_∞ attacks.

DBP method	Dataset	Vanilla			ADDT			ADDT_{l_∞}		
		Clean	l_∞	l_2	Clean	l_∞	l_2	Clean	l_∞	l_2
DP_{DDPM}	CIFAR-10	85.94	47.27	69.34	85.64	51.46	**70.12**	84.47	**52.64**	68.55
	CIFAR-100	57.52	20.41	37.89	59.18	**23.73**	**41.70**	57.81	23.24	40.04
DP_{DDIM}	CIFAR-10	88.38	42.19	70.02	88.77	46.48	**71.19**	88.48	**50.49**	70.31
	CIFAR-100	63.28	15.23	36.62	66.02	18.85	**39.84**	64.84	**20.31**	39.36

M Additional Experiments under Deterministic White-box Setting

Evaluation across different NFEs We also investigate the robustness under the Deterministic White-box Setting across varying NFEs. The comparison of performance between vanilla models and ADDT fine-tuned models, shown in Figure 11, highlights that ADDT consistently enhances model performance at different NFEs. This improvement is particularly pronounced at lower NFEs, further confirming that ADDT enables diffusion models to more effectively counter adversarial perturbations.

Table 22: DW-box accuracy (%) under ℓ_∞ perturbations for various models. ADDT consistently improves robustness across all models.

DBP method	Vanilla	ADDT
DP_{DDPM}	16.80	**39.16**
DP_{DDIM}	4.98	**17.09**
DiffPure	22.76	**51.63**
DP_{EDM}	13.33	**32.94**

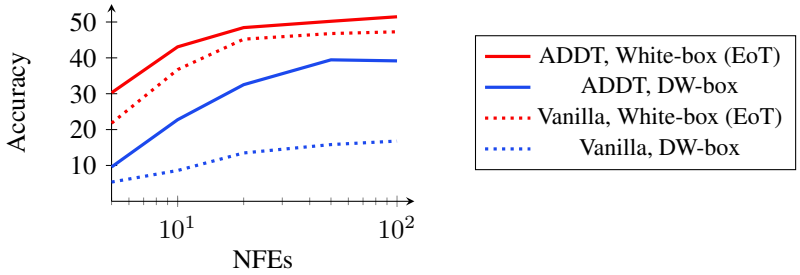

Figure 11: Revisiting Deterministic White-box Robustness. ADDT consistently improves robustness under both White-box and Deterministic White-box setting, implying that ADDT strengthens the models' ability to handle adversarial inputs.

N Sensitivity Analysis of λ_{unit}

In Section 6.1 we choose λ_{unit}=0.03 as the magnitude of such noise is similar to the adversarial pertubation of common adversarial attack setting. We also provide an ablation study here, which shows that the performance of ADDT is insensitive to λ_{unit} and gets a consistent improvement.

Table 23: The performance of ADDT fine-tuned DP_{DDPM} with varying λ_{unit} values. ADDT shows insensitivity to λ_{unit} and consistently improves robust accuracy (%).

NFEs	l_∞				ℓ_2			
	Vanilla	0.02	0.03	0.04	Vanilla	0.02	0.03	0.04
5	21.78	24.02	30.27	**31.25**	36.13	41.99	41.99	**49.02**
10	36.72	40.92	43.07	**44.92**	55.47	61.72	62.97	**64.45**
20	45.21	48.14	48.44	**50.68**	65.23	67.48	**69.82**	69.24
50	46.78	48.83	50.20	**51.07**	68.85	**69.82**	69.04	69.53
100*	47.27	48.93	**51.46**	50.88	69.34	**70.31**	70.12	69.92

O Computational Cost Analysis for Training and Inference

Fine-tuning DDPM and DDIM models using ADDT to achieve near-optimal performance requires 50 epochs and approximately 12 hours of training on 4 NVIDIA GeForce RTX 2080 Ti GPUs. This efficiency matches that of traditional adversarial training approaches and is notably faster than recent adversarial training techniques that utilize diffusion models for dataset augmentation (Wang et al., 2023). However, testing DP_{DDPM} and DP_{DDIM} involves significant computational expense due to the use of Expectation over Transformation (EoT). For instance, validating 1,024 images on the CIFAR10/CIFAR100 datasets takes approximately 5 hours on the same GPU configuration.

One of the key advantages of ADDT is its "train-once" methodology. Once the initial training is complete, ADDT can protect multiple classifiers without requiring additional fine-tuning, as demonstrated in Table 2. This is in stark contrast to adversarial classifier training, where each classifier demands individual training.

During inference, models trained with ADDT have a similar complexity to standard DBP. However, their performance gains in accelerated scenarios offer the potential for a reduction in computational overhead. As shown in Table 4, DP_{DDPM} + ADDT achieves comparable performance to DP_{DDPM} while requiring only 20 NFEs, resulting in up to an 80% reduction in computation time compared to the 100 NFEs required for DP_{DDPM}.

P Credibility of Our Paper

The code was developed independently by two individuals and mutually verified, with consistent results achieved through independent training and testing. The open-source code is available at https://github.com/LYMDLUT/ADDT.

Q Broader Impact and Limitations

Our work holds significant potential for positive societal impact across a range of sectors, including autonomous driving, facial recognition payment systems, and medical assistance. We are dedicated to enhancing the safety and trustworthiness of global AI applications. However, we acknowledge the potential negative societal impacts, particularly concerning privacy protection, due to adversarial perturbations. Despite this, we believe that the overall positive impacts outweigh these risks.

In terms of limitations, our approach could benefit from incorporating insights from traditional adversarial training methods (Zhang et al., 2019; Shafahi et al., 2019; Wang et al., 2023), such as through more extensive data augmentation and a refined ADDT loss design. Nevertheless, these limitations are relatively minor and do not diminish the overall contributions of this paper. We believe these new findings and perspectives will have a sustained impact on future research in DBP, which is a promising approach to adversarial defense and could prove even more valuable for real-world applications, despite the early stage of existing studies on DBP.